Redox Biology 88 (2025) 103900

Contents lists available at ScienceDirect

Redox Biology

journal homepage: www.elsevier.com/locate/redox

Geniposide, a potential therapeutical candidate for acute pancreatitis, inhibited trypsinogen-activated CBS degradation and remodeled transsulfuration metabolic flux

Ji Gao [a,1], Yijing Long [b,1], Jiawang Li [a], Yiqin Wang [a], Rui Wang [b], Jinxi Yang [a], Jie Zhang [c], Chenxia Han [a], Qing Xia [a,*], Dan Du [a,b,**]

[a] West China Center of Excellence for Pancreatitis, Institute of Integrated Traditional Chinese and Western Medicine, West China Hospital, Sichuan University, Chengdu, 610041, China
[b] Advanced Mass Spectrometry Center, Research Core Facility, Frontiers Science Center for Disease-related Molecular Network, West China Hospital, Sichuan University, Chengdu, 610213, China
[c] ChengDu Institute for Drug Control, SCMPA Key Laboratory for Quality Research and Control of Chemical Medicine, Chengdu, 610045, China

ARTICLE INFO

Keywords:
Acute pancreatitis
Geniposide
Trypsinogen activation
Cystathionine β-synthase
Post-translational modifications
Metabolic reprogramming

ABSTRACT

Acute pancreatitis (AP) is a potentially fatal condition with no targeted treatment options currently available. The premature activation of trypsinogen within acinar cells constitutes one of the pivotal early pathological events in AP, contributing to oxidative stress and inflammation. Disruption of the transsulfuration pathway also plays an important role in the development of AP. However, the interplay between these factors remains unclear. Here, we found that geniposide (GE), isolated from *Gardenia jasminoides J. Ellis*, ameliorated pancreatic acinar cell injury while exhibiting profound antioxidant activity both *in vitro* and *in vivo*. Then, we observed disrupted cysteine and methionine metabolism, manifested as reduced metabolic flux for cysteine and glutathione synthesis as well as increased toxic hydrogen sulfide in injured pancreatic acinar cells, all of which could be restored by GE treatment. Moreover, we revealed that cystathionine β-synthase (CBS), the rate-limiting enzyme of the transsulfuration pathway, undergoes cleavage by trypsin in injured pancreatic acinar cells and is responsible for the aforementioned metabolic reprogramming. Notably, GE stabilized the full-length CBS from cleavage primarily by suppressing trypsinogen activation and reducing the post-translational modification of truncated CBS forms, rather than through the direct, weak, and allosteric interactions. Our study is the first to highlight that early trypsin activation influences the proteolysis of metabolic enzymes, thereby affecting metabolic reprogramming and exacerbating the severity of AP. Additionally, we provide GE as a natural product candidate for preventing disease progression.

Abbreviations: AP, acute pancreatitis; GE, geniposide; CBS, cystathionine β-synthase; GSH, glutathione; H_2S, hydrogen sulfide; SAM, s-adenosylmethionine; CER, cerulein; NaT, sodium taurocholate hydrate; GSSG, oxidized glutathione; GPx, glutathione peroxidase; SOD, superoxide dismutase; MPO, myeloperoxidase; ROS, reactive oxygen species; mBBr, monochlorobimane; B-SG, GSH-monochlorobimane; AzMC, 7-azido-4-methylcoumarin; AMC, 7-amino-4-methylcoumarin; RT-qPCR, reverse transcription-quantitative polymerase chain reaction; WB, western blotting; ELISA, enzyme-linked immunosorbent assay; SDS-PAGE, sodium dodecyl-sulfate polyacrylamide gel electrophoresis; LiP-MS, limited proteolysis-mass spectrometry; H&E, hematoxylin and eosin; KEGG, kyoto encyclopedia of genes and genomes enrichment; VIP, variable importance in projection; TAP, trypsinogen activation peptide; CTSB, cathepsin B; CSE, cystathionine γ-lyase; SEM, standard error of the mean.

* Corresponding author.
** Corresponding author. West China Center of Excellence for Pancreatitis, Institute of Integrated Traditional Chinese and Western Medicine, West China Hospital, Sichuan University, Chengdu, 610041, China.
E-mail addresses: xiaqing@medmail.com.cn (Q. Xia), dudan1520@163.com (D. Du).
[1] These authors contributed equally to this work.

https://doi.org/10.1016/j.redox.2025.103900
Received 8 August 2025; Received in revised form 27 September 2025; Accepted 15 October 2025
Available online 16 October 2025

1. Introduction

Acute pancreatitis (AP) is an acute inflammatory disorder of the pancreas, characterized by damage to pancreatic acinar cells and inflammatory cell infiltration. It can progress to systemic inflammatory response syndrome and persistent multiple organ failure in a short period but lacks targeted therapeutic drugs, resulting in a high mortality of 20 %–40 % [1]. Thus, the development of drugs for the management of pancreatic injuries is crucial for preventing disease progression. Multiple pathophysiological mechanisms of pancreatic acinar cells have been reported for contributing to AP, including premature activation of trypsinogen, calcium overload, mitochondrial dysfunction, oxidative stress, endoplasmic reticulum stress, ferroptosis, etc [2]. Notably, metabolic disruption and reprogramming elaborately inter-connecting with the aforementioned cellular pathological processes, significantly influence the progression of AP and are currently considered to be the most promising therapeutic target for AP [3,4].

Disorders in methionine and *trans*-sulfuration metabolism constitute a critical factor in the pathogenesis and progression of AP. The young and female mice fed with a choline-deficient diet supplemented with 0.5 % DL-ethionine could induce hemorrhagic pancreatic necrosis [5]. Transsulfuration pathway defects and glutathione (GSH) depletion are associated with progression to severe attacks [6]. In detail, cystathionine β-synthase (CBS) nitration and blockade partly impair homocysteine metabolism and limit the metabolic flux through the *trans*-sulfuration pathway. However, as an important allosteric regulator of CBS, supplementation of S-adenosylmethionine (SAM) did not ameliorate but rather exacerbated AP in this study [7]. In fact, CBS is not only acting as a rate-limiting enzyme in transsulfuration for the degradation of homocysteine and forming cystathionine but also responsible for the production of hydrogen sulfide (H_2S), an inflammation mediator during AP [8,9]. Therefore, whether alterations in CBS enzyme activities affect metabolic reprogramming and further exacerbate AP warrants deeper study.

Traditional Chinese medicine has demonstrated considerable efficacy in the treatment of exocrine pancreatic disorders [10,11]. Geniposide (GE), a natural iridoid glycoside, is mainly isolated from *Gardenia jasminoides J. Ellis* [12]. It has demonstrated a wide range of curative effects in several inflammatory diseases, such as hepatic injury, colitis, arthritis, etc, owing principally to its anti-inflammatory and antioxidant effects [12]. GE also serves as a critical quality-marker in Chaiqin Chengqi Decoction, a clinically effective formula, with its content variation demonstrating a positive correlation with the *anti*-AP efficacy of the formula [13]. Abnormal alterations in CBS expression and cystathionine levels have also been observed in our previously established time-course AP mice model, which could be partly restored by Chaiqin Chengqi Decoction [14]. However, the underlying regulatory mechanism remains unclear, and it is unknown whether GE serves as the primary effective component responsible for improving *trans*-sulfuration and alleviating AP.

In this study, firstly we evaluated the protective effects of GE on AP *in vitro* and *in vivo*; then we studied its metabolic regulation in *trans*-sulfuration on an experimental AP model using metabolomics and confirmed by metabolic flux in pancreatic acinar cells; furthermore, we disclosed interactions between GE and CBS as well as the regulation of GE on CBS activity and the post-translational modification of CBS proteolytic cleavage; lastly, we analyzed the catalytic activity of proteolytic CBS on H_2S generation and the effect of GE on proteolytic degradation. Taken together, GE reprogrammed the transsulfuration metabolism to enhance the synthesis of GSH and decrease the generation of H_2S by inhibiting trypsinogen-activated post-translational modification of cleaved CBS and its enzyme activity rather than through the direct molecular interactions, finally conferring antioxidant effects and protection against AP both *in vivo* and *in vitro*. GE is a promising natural leading compound with significant therapeutic potential for the treatment of early AP and warrants further development.

2. Materials and methods

A detailed description of the *Information for antibodies, chemicals, assay kits, and software* (Supplementary Table S1), *Cell death assay*, *Lactate dehydrogenase release assay*, *Cellular trypsin activity assay, Reverse transcription-quantitative polymerase chain reaction (RT-qPCR)*, *Western blotting (WB)*, *Immunohistochemistry, Immunofluorescence, Enzyme-linked immunosorbent assay (ELISA),* and *Targeted metabolomics analysis in pancreatic acinar cells* can be found in the **Supplementary Materials and Methods**.

2.1. Ethics, human sample collection, and animals

2.1.1. Human studies and blood sample collections

All human studies adhered to the principles outlined in the Declaration of Helsinki, designed according to the TRIPOD guidelines [15]. The studies received approval from the Institutional Review Board and Biomedical Ethics Committee of West China Hospital, Sichuan University (approval number: 2020, no. 196; 2020, no. 107). Written informed consent was obtained from all patients and healthy volunteers (HV) or their legal guardians before blood sampling. Biobanking procedures, clinical data collection, and storage followed our previous study [16].

The basic inclusion and exclusion criteria were reported according to our previous study [17]. Briefly, inclusion criteria were: (1) age, 18 − 75 years old; (2) meet the diagnostic criteria of the AP; (3) admitted to the hospital within 48 h of onset. Patients who are in advanced or end-stage pulmonary, cardiac, renal diseases, liver cirrhosis, malignancy, pregnancy, lactation, or re-admission during the same episode of AP were excluded. The AP severity of patients was categorized by the revised Atlanta classification [18]. Peripheral blood samples were obtained from AP patients who presented to our hospital within 72 h of abdominal pain onset. Plasma samples from healthy volunteers were obtained from the West China Biobanks. Blood was collected in ethylenediaminetetraacetic acid tubes for plasma determination. The clinical information for samples is noted in Supplementary Table S2.

2.1.2. Animals and experimental models

All animal experiments were approved by the Animal Ethics Committee of West China Hospital, Sichuan University (approval number: 20230218006). Male C57BL/6J mice (22–25 g) were purchased from Beijing Huafukang Biotechnology Co., Ltd. or Jiangsu Gempharmatech Co., Ltd. Animals were maintained at 21 ± 2 °C with a 12 h light-dark cycle and ad libitum feeding of standard laboratory chow and water throughout the experiment.

Cerulein-induced AP (CER-AP) mouse model was employed in our study: AP was induced by 7 hourly intraperitoneal injections of CER (50 μg/kg body weight, i.p.), while control groups received intraperitoneal phosphate-buffered saline injections of the same volume at the same intervals. The first CER injection was labeled as 0 h.

For treatment with GE, (1) GE was administered with simultaneous CER modeling: Mice were intravenously injected with GE at 14 mg/kg simultaneously with the second CER injection at time points 1, 4, and 7 h (2) Administration totally after CER-AP modeling: mice were administered GE at a dose of 14 mg/kg immediately after 7 times CER injections, followed by 3 intravenous injections via the tail every 2 h (6, 8, and 10 h).

Blood, pancreas, and lung tissues were taken 12 h after receiving the first CER injection. Serum was used for the measurement of amylase, lipase, GSH/oxidized glutathione (GSSG), glutathione peroxidase (GPx), and superoxide dismutase (SOD) enzyme activities. The entire pancreas was promptly removed. Separated pancreas was utilized to test GSH/GSSG, reactive oxygen species (ROS), trypsin activity, myeloperoxidase (MPO) activity, histological assessment, WB, RT-qPCR, immunohistochemistry, or non-targeted metabolomics analyses. Lung tissues were also isolated for MPO measurement. Except for histological samples, which were kept in 10 % neutral formaldehyde, all samples were

aliquoted and frozen at −80 °C for usage.

2.2. AP severity indicators

Serum amylase, serum lipase, pancreatic MPO activity, lung MPO activity, and pancreatic trypsin activity levels were measured as previously reported [19]. Established scoring criteria were used for pancreatic histopathology assessment, including pancreatic edema, inflammatory cell infiltration, and cell necrosis [20].

2.3. Isolation of pancreatic acinar cells

Pancreatic acinar cells were freshly isolated from mice by collagenase IV digestion using our established methods [19].

2.4. Measurement of reduced GSH, reduced GSH/oxidized GSSG, SOD, and GPx levels in pancreatic acinar cells, serum, and pancreas

2.4.1. Cellular GSH assay

GSH was detected by using a monochlorobimane probe (mBBr, 20 μM) at 37 °C for 30 min in the dark. The mBBr reacted with GSH to form a fluorescent GSH-monochlorobimane (B-SG) adduct which was detected by fluorescence microscopy at Ex/Em = 380/465 ± 20 nm respectively (blue) [21]. Pancreatic acinar cells were pre-incubated with GE (100 μM) and sodium taurocholate hydrate (NaT) (4 mM) in the HEPES buffer for 30 min, followed by mBBr-staining for another 30 min. Then the dye and treatment were removed by centrifugation. The cells were imaged via Andor Dragonfly 200 confocal microscope (Andor Technology, Belfast, UK) or Leica DMI8 fluorescent microscopy (Leica, Wetzlar, Hesse, DE) as soon as they were resuspended. The relative fluorescence intensity of GSH in pancreatic acinar cells was quantified by Image J. For the fluorescence microplate reader (BioTek-Cytation 5, Winooski, VT, USA), the fresh cell suspension, after removal from mBBr-stained, was incubated with NaT (4 mM) and GE (100 μM) in a total volume of 200 μL HEPES buffer per well with time-course fluorescence recording.

2.4.2. Measurement of reduced GSH and reduced GSH/oxidized GSSG in serum and pancreas of AP mouse models

The ratio of reduced GSH and oxidized GSSG of pancreas and serum was measured by LC-MS/MS (AB Sciex 6500 Plus, Framingham, MA, USA). For sample preparation, N-Ethylmaleimide was added to inhibit glutathione reductase to prevent changes in GSSG levels. Approximately 10 mg of frozen pancreas samples were homogenized with 500 μL of 80 % methanol including 6.25 mg/mL N-Ethylmaleimide, and incubated for 30 min at 4 °C. The homogenization buffer was centrifuged, the supernatant was dried, and then reconstituted with 100 μL of H_2O (4 μL was injected). For the serum preparation, 100 μL of the sample was precipitated by 1 mL of 80 % methanol, and 1 mL of supernatant was dried and reconstituted in 100 μL of H_2O (2 μL was injected). To calculate the GSH contents of the pancreas, a series of known concentrations of GSH standard solutions (5 ng/mL - 1000 ng/mL) was prepared for fitting the standard curve. For serum samples, different linear portions (1 ng/mL - 1000 ng/mL for GSH and 250 ng/mL - 800 ng/mL for GSSG) were performed. Nexera LC-30A UHPLC system (Shimadzu, Kyoto, Japan) equipped with a Waters BEH Amide column (2.1 mm × 100 mm x 1.7 μm; Waters, Milford, MA, USA) was used for the metabolites separation. Mobile phase A was 10 mM ammonium acetate and 0.2 % acetic acid in 10 % acetonitrile, while mobile phase B was 90 % acetonitrile. The column was maintained at 40 °C, and the flow rate was 0.3 mL/min. The mobile phase gradient was set as follows: 1.5 min, 90 % of B; 5 min, 45 % of B; 10 min, 45 % of B; 12 min, 90 % of B; 25 min, 90 % of B. The AB Sciex triple quadrupole 6500 Plus mass spectrometer (AB Sciex, Framingham, MA, USA) was used for metabolite detection using MRM. The source temperature was kept at 400 °C. Metabolites were identified based on standard retention times, with peak detection using SCIEX OS software.

2.4.3. Serum GPx and SOD in AP

The enzyme activities of GPx and SOD in serum were assessed by commercial kits of Nanjing Jiancheng according to the manufacturer's instructions.

2.5. Measurement of ROS levels

2.5.1. Cellular ROS levels

Pancreatic acinar cells were pre-incubated with a ROS probe H2-DCFDA (10 μM) for 30 min at room temperature in the dark, as previously described [22]. On the one hand, removal from the dye, cells with modeling agents (NaT, 4 mM; H_2O_2, 150 μM) and GE (100 μM) were time-course measured for ROS levels using a microplate reader (BioTek-Cytation 5, Winooski, VT, USA). On the other hand, the probe, GE (100 μM), and NaT (4 mM) were co-incubated with pancreatic acinar cells for exactly 1 h, then the cells were captured by the Andor Dragonfly 200 confocal microscope (Andor Technology, Belfast, UK). The relative fluorescence intensity of ROS was quantified by Image J.

2.5.2. Pancreatic ROS expression of AP samples

Pancreatic ROS levels of the paraffin sections were measured with a ROS assay kit as reported methods [23]. In summary, the cleaning solution was used for paraffin sections, followed by a 200 μL ROS fluorescent probe. Then the sections were incubated at 37 °C for 40 min in the dark with PBS cleaning 3 times after that. Fluorescence images were captured by a fluorescence microscope (Olympus-VS200, Tokyo, Japan) and analyzed by Image J.

2.6. Non-targeted metabolomics analysis in the pancreas

A total of 24 pancreatic samples from Ctrl, CER-AP, and GE groups (n = 8 per group) were included. A pooled tissue sample was used as the QC sample. Approximately 10 mg of the pancreas was homogenized with 200 μL of 50 % methanol and then diluted with 300 μL of 50 % methanol. The supernatant was collected after vortexing, quenching, and centrifuging. Another 500 μL of 50 % acetonitrile was added for the second extraction, followed by supernatant combination and concentration. Subsequently, the extracted metabolites were derivatized with methoxyamine (45 μL, 20 mg/mL) dissolved in pyridine for 2 h and with 60 μL of *N*-methyl-*N*-trimethylsilyl-trifluoroacetamide (with 1/31 fatty acid methyl esters) for 1.5 h. One μL of supernatant was then analyzed by an Agilent 8890 GC (Agilent, Santa Clara, CA, USA)/Leco Pegasus BT TOFMS (Leco, St. Joseph, MI, USA) with a Rxi-5ms column (30 m × 0.25 mm x 0.25 μm; Restek, Bellefonte, PA, USA). The oven temperature programs were set as follows: initial 70 °C (held for 22 min), then increased to 130 °C at 20 °C/min (held for 1 min), and next changed to 10 °C/min until 310 °C (held for 6 min). The temperature of the splitness injector was 250 °C. The ion source and transfer line temperatures were 250 °C and 280 °C, respectively. The mass detector was performed by full scan mode, ranging from 85 to 550 amu, and the electron ion source was 70 eV. Raw Spectrum was processed by Pegasus BT Software, and data correction was performed by QC samples and protein concentration, followed by normalization through the Wukong platform (http://www.omicsolution.org/wu-kong-beta-linux/main/). The significant metabolites were analyzed as previously described with similar screen criteria ($P < 0.05$ and variable importance in projection (VIP) score >1) [14].

2.7. Cell metabolic flux analysis

The analysis was conducted as our established methods [23]. Cells for the [$^{13}C_3$]-serine tracing and [$^{13}C_5$]-methionine tracing were prepared in the same way as previously described [23], but the HEPES buffer contained certain stable isotope-labeled metabolites ([$^{13}C_3$]-serine, 400 μM; [$^{13}C_5$]-methionine, 200 μM). Pancreatic acinar cells were isolated freshly and divided into three groups (Ctrl, AP, and

GE) with three replicates. Before extraction, cells were fed with [$^{13}C_3$]-serine or [$^{13}C_5$]-methionine for 1 h. Metabolites were extracted using 80 % methanol with 25 mM N-Ethylmaleimide. Post-quenching, cells were incubated at 4 °C for 30 min, followed by centrifugation (17000 g, 20 min, 4 °C). The supernatant was dried, reconstituted in 70 % acetonitrile, and analyzed by LC-MS/MS (AB Sciex 6500 Plus, Framingham, MA, USA). The instrument conditions were identical to the measurement of reduced GSH. Isotope correction for the extracted metabolite intensities was performed using the IsoCorrectoR 1.20.0 package with normal resolution correction [24].

2.8. Assessment for H_2S

2.8.1. CBS enzyme activity for H_2S assay

The measurement of CBS enzyme activity was performed using a commercial cystathionine beta-synthase assay kit with a microplate detection system (PerkinElmer, Waltham, MA, USA). The assay kit specifically measures H_2S production. CBS enzyme activities for pure recombinant CBS, pancreatic acinar cells, and human plasma were similarly measured according to the manufacturer's recommendations of the kit. For defining the direct impacts of GE on full-length and cleaved CBS, GE (50, 100, and 200 μM) was co-incubated with CBS proteins for 30 min. For validating the effects of trypsin on full-length CBS, concentrations of trypsin (TPCK-treated, 1, 5, 10, and 20 nM; 50, 100, and 200 nM) and full-length CBS were incubated for 1 h, followed by TLCK (1 mM) quenching [25]. The suspension was then added to the CBS enzyme activity assay. Regarding the modulation of GE on CBS activity under trypsin conditions, GE (200 and 400 μM) with full-length recombinant CBS was thoroughly pre-incubated, followed by trypsin (10 nM) being added into the solution system for proteolytic reaction. On the other hand, GE (200 and 400 μM) was pre-incubated with trypsin (10 nM), with full-length CBS subsequently added. Finally, the suspension was acquired for the enzyme activity assay. Besides, human plasma from clinical populations and the supernatant of cell samples that were co-incubated with NaT and GE for 1 h could be directly used for H_2S measurements characterized by the CBS enzyme activity assay.

2.8.2. Other assays

H_2S fluorescence image in pancreatic acinar cells was also traced by the 7-azido-4-methylcoumarin (AzMC, 50 μM) fluorescence probe at the Ex/Em = 365/450 nm, as per the manufacturer's recommendations. Cells were pre-incubated with GE (100 μM) for 30 min, followed by probe and NaT (4 mM) addition, and further incubated for another 1 h with time-course fluorescence recording by the microplate reader or imaging captured at the final time point using the Andor Dragonfly 200 confocal microscope (Andor Technology, Belfast, UK). Imaging was analyzed by Image J. For the serum H_2S of mice, a commercial H_2S assay kit from Nanjing Jiancheng was used for detection.

2.9. CBS enzyme activity on cystathionine detection from cysteine or serine

For cystathionine determination, the reaction mixtures from the cystathionine beta-synthase assay kit were first precipitated with 500 μL of pre-cooled 80 % methanol. The supernatants were collected, dried, and reconstituted in 100 μL of 70 % acetonitrile. A 10 μL aliquot of the reconstitution solution was then desalted using a Nexera LC-40 system equipped with an FRC-40 fraction collector (Shimadzu, Kyoto, Japan), applying the same chromatographic separation conditions as those used for measuring reduced GSH. The fraction containing cystathionine was finally collected and analyzed by LC-MS/MS (AB Sciex 6500 Plus, Framingham, MA, USA) using parameters identical to those for GSH quantification. For the determination of labeled cystathionine derived from [$^{13}C_3$]-serine (30 mM) spiked into the CBS assay, the same workflow as for unlabeled cystathionine was followed.

2.10. Limited proteolysis-mass spectrometry (LiP-MS) analysis

The purified full-length CBS protein (10 μg) was incubated with GE at 100 μM, and a control group without GE was prepared. The incubation was performed at 25 °C for 30 min. Next, proteinase K was added to each sample at a proteinase K/protein ratio of 1:100 (w/w) and incubated at 25 °C for 5 min. The limited proteolysis was terminated by heating the samples at 98 °C for 5 min in a thermocycler, followed by the addition of sodium deoxycholate to a final concentration of 5 %. 10 mM dithiothreitol was then added to incubate for 1 h at 56 °C. Then, the alkylation was achieved by adding iodoacetamide to a final concentration of 25 mM for 30 min at 25 °C in the dark. Samples were treated with freshly prepared 100 mM ammonium bicarbonate to a final concentration of 1 % sodium deoxycholate and were predigested with lysyl-endopeptidase at an enzyme/substrate ratio of 1:100 (w/w). After 2 h incubation at 37 °C, samples were reacted with trypsin at an enzyme/substrate ratio of 1:100 (w/w) at 37 °C for 16 h. The reaction was quenched by adding 10 % (v/v) trifluoroacetic acid to lower the PH (< 3). The acidified peptide mixtures were loaded onto a C18 microspin cartridge, desalted, and eluted using a solution of 50 % acetonitrile and 0.1 % trifluoroacetic acid. Following elution, the peptides were dried using a vacuum centrifuge, resuspended in 0.1 % formic acid, and subsequently analyzed by an Orbitrap Exploris 480 mass spectrometer (Thermo Fisher Scientific, Waltham, MA, USA). Acquired data-independent acquisition data were searched by Spectronaut 19.9 (Biognosys AG, Zurich, Switzerland). Prior to comparing the relative abundance, the dataset underwent median normalization and was filtered to retain only proteotypic peptides. The final output of the statistical analysis was filtered based on the following criteria: $P < 0.05$ and $|\log_2 FC| > 1.5$.

2.11. Cellular thermal shift assay

Cellular thermal shift assay was performed following the reported studies [23]. Briefly, isolated pancreatic acinar cells were incubated with NaT (2 mM) for 1 h, then resuspended in RIPA and equally transferred into tubes. Protein concentration was measured by the bicinchoninic acid protein assay kit. Then the protein concentration was adjusted to 1 μg/μL with H_2O, split evenly between 2 tubes, and further incubated with GE (100 μM) or the same volume of H_2O for 1 h, respectively. After the incubation, the mixture was partitioned into 50 μL aliquots within individual tubes and subjected to heating for a duration of 5 min at the specific temperature (58, 60, 62, 64, 66, and 68 °C, respectively). After cooling, the samples were centrifuged to get the supernatant, and then sodium dodecyl-sulfate polyacrylamide gel electrophoresis loading buffer was incorporated into it for denaturation, which was subsequently analyzed and repeated by WB at least 3 times.

2.12. Expression and purification of recombinant CBS

We purified recombinant CBS using the detailed methods described previously [26]. The constructs full-length CBS (residues 1–551) and cleaved CBS (residues 1–413) were confirmed by sequencing. The sequence-optimized CBS was synthesized and inserted into pET28a at the sites of *Nde*I and *Sal*I. The resulting plasmid pET28a-CBS was transformed to *E. coli* transetta for GST-tagged or 6xHis-tagged CBS fusion protein expression. *E. coli* was incubated into 2 L flasks containing 1 L LB media and cultivated at 37 °C and 220 rpm. To induce the protein expression, the temperature was timely lowered to 16 °C using 60 μM IPTG when the OD600 reached 0.4–0.6. The bacterial sludge was obtained through centrifugation and subsequently resuspended in 75 mL of A + 10 buffer to facilitate cell disruption using a high-pressure homogenizer (ATS Engineering Limited, Cambridge, ON, Canada). Soluble supernatant was applied to 1 mL Ni-NTA agarose for Ni-affinity purification after centrifugation at 4 °C and 14000 rpm for 40 min. The nonspecific binding proteins were eliminated using 45-column volumes

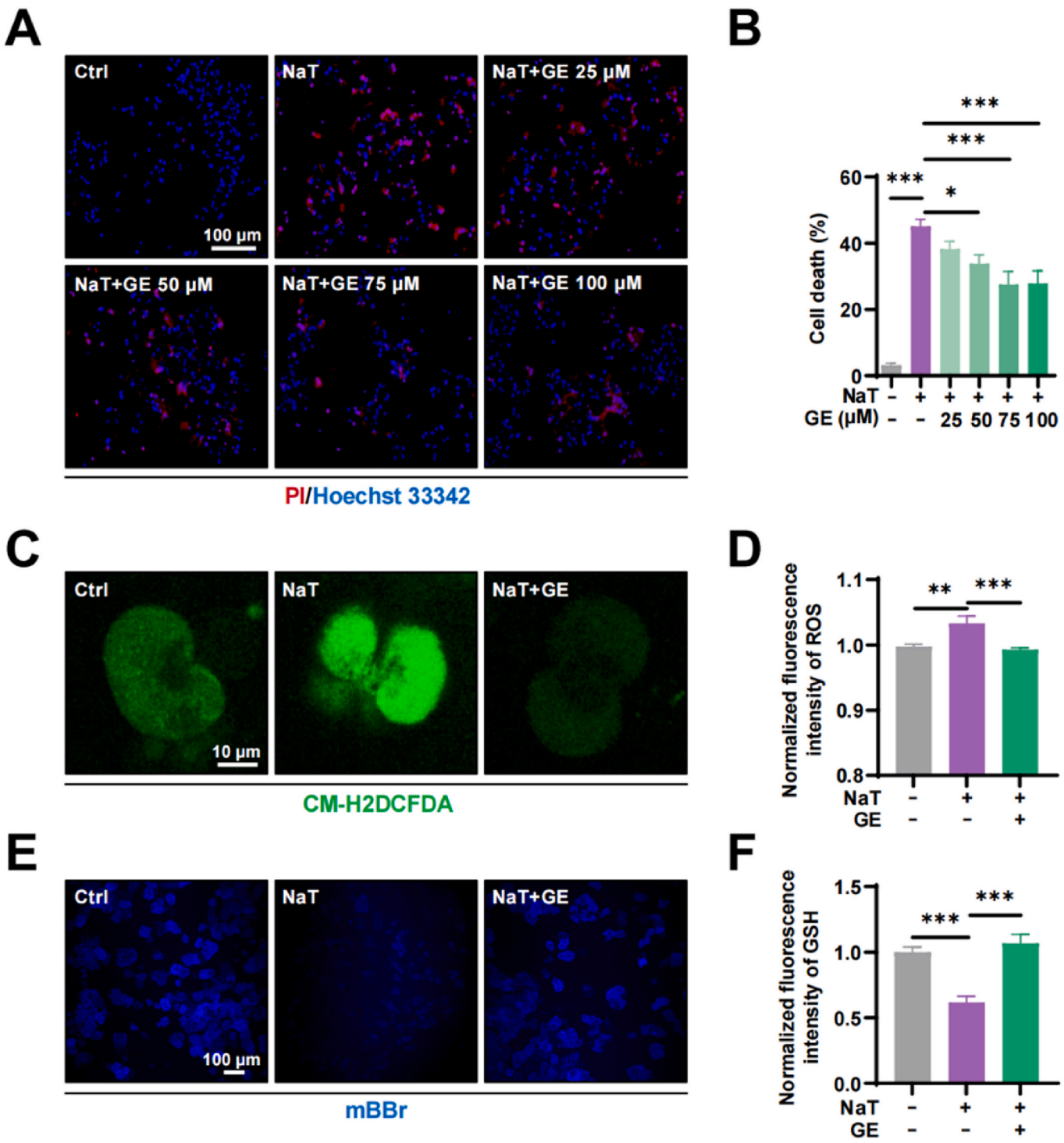

Fig. 1. GE reduced necrosis and oxidative stress in pancreatic acinar cells stimulated by NaT. (A) Representative images for the protective effects of GE on necrotic cell death activation under NaT exposure. (Blue, Hoechst 33342; red, PI. Bar = 100 μm). (B) Quantitative results of necrosis in three groups ($n = 6$ ROIs). (C) Fluorescence images for the effects of GE (100 μM) on ROS generation in pancreatic acinar cells stimulated by NaT. (Green, CM-H2DCFDA. Bar = 10 μm). (D) Quantitative analysis of the fluorescence intensity (normalized to Ctrl) for ROS in three groups ($n = 25$–30 cell clusters). (E) Fluorescence staining for GSH in NaT-induced pancreatic acinar cells with GE (100 μM) therapy by using a monochlorobimane probe. The monochlorobimane reacted with GSH to generate B-SG, which was detected by fluorescence microscopy at 470 nm. (Blue, mBBr. Bar = 100 μm). (F) Quantitative analysis for the fluorescence intensity (normalized to Ctrl) of GSH characterized by B-SG among the three groups ($n = 8$ ROIs). Data are presented as mean ± SEM; $^{*}P < 0.05$, $^{**}P < 0.01$, and $^{***}P < 0.001$.

of A + 20 buffer and 30-column volumes of A + 50 buffer. Then the Nickel chelating proteins were washed from the resin by 15 mL A + 250 buffer. The elution fractions containing target CBS were concentrated to 2.5 mL with a centrifugal device (Amicon-50K MWCO, Billerica, MA, USA) and then placed onto a disposable PD-10 desalting column (GE Pharmacia, Chicago, IL, USA), washed with 3.5 mL water for desalting. Finally, the proteins were concentrated and subsequently exchanged into a storage buffer utilizing a 10 kDa ultrafiltration cube. The purity of recombinant CBS was determined by sodium dodecyl-sulfate polyacrylamide gel electrophoresis, and the concentration was measured

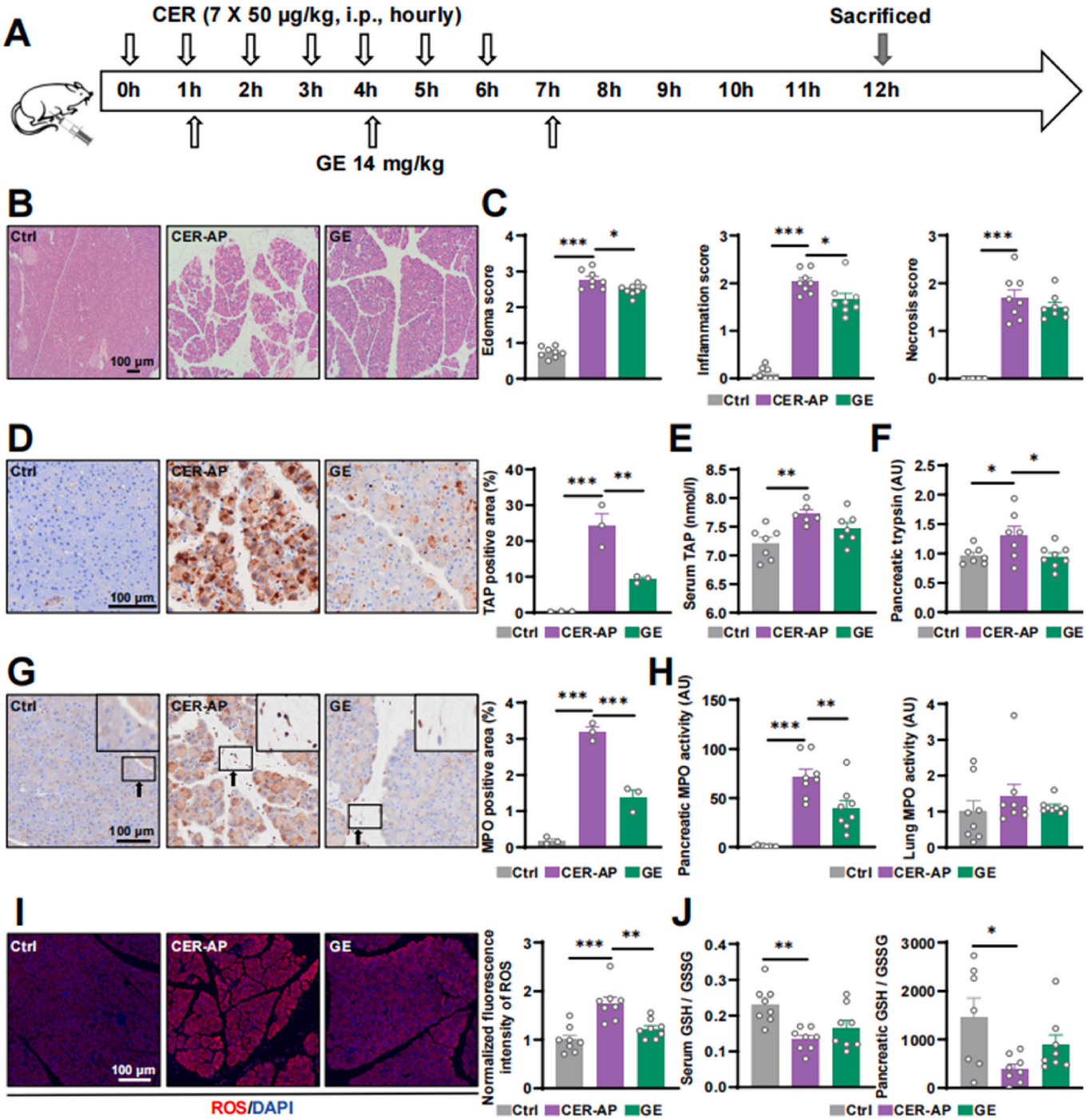

Fig. 2. GE therapy with concomitant CER induction ameliorated trypsinogen activation, oxidative stress, and pancreatic injury in CER-AP mouse models. (A) Schematic illustration of animal experiments with all the time points on GE (14 mg/kg) treatments at 1, 4, and 7 h with concomitant the second CER stimulation. (B) Representative hematoxylin and eosin (H&E) images for the pancreas of CER-AP mice. (Bar = 100 μm). (C) Histological scores of edema, inflammation, and necrosis ($n = 8$). (D) Representative images and quantitative results of immunohistochemical staining for trypsinogen activation peptide (TAP) expression in Ctrl, CER-AP, and GE groups (Bar = 100 μm. $n = 3$). (E) Serum TAP levels in the three groups ($n = 6$–7). (F) The inhibition of GE on pancreatic trypsin activity for CER-AP mice ($n = 7$–8). (G) Representative immunohistochemical staining for pancreatic MPO expression and its quantification results (Bar = 100 μm. $n = 3$). (H) The ameliorative effects of GE on pancreatic and lung MPO activity for CER-AP mice ($n = 8$). (I) Representative images and quantification results (normalized to Ctrl) of pancreatic ROS expression in Ctrl, CER-AP, and GE groups. (Blue, DAPI; red, ROS. Bar = 100 μm. $n = 8$). (J) The ratio of GSH/GSSG in serum and pancreas from three groups ($n = 7$–8). Data are presented as mean ± SEM; $^{*}P < 0.05$, $^{**}P < 0.01$, and $^{***}P < 0.001$.

using a Bradford assay kit.

2.13. Sodium dodecyl-sulfate polyacrylamide gel electrophoresis (SDS-PAGE)

The SDS-PAGE profile was conducted using the described method [27]. The gel preparation and electrophoresis steps for SDS-PAGE were

consistent with the WB protocol in the **Supplementary Materials and Methods**. Sample preparations matched the enzyme activity assay for recombinant CBS proteins. After electrophoresis, the gel was stained and destained with the eStain L1 kit, finally being imaged for analysis. The molecular weights of proteins were determined by running the protein markers in parallel on the same gel.

2.14. Microscale thermophoresis binding assay

The Microscale thermophoresis binding assay using Monolith NT.115 (NanoTemper, Munich, Bavaria, DE) was performed as established previously [28]. The recombinant CBS protein was labeled using the Monolith series protein labeling kit, which was subsequently combined with samples containing various concentrations of GE. GE was serially diluted in 2-fold steps starting from 500 μM. The mixed solution was aspirated with a capillary and loaded for detection. Then the binding affinity between GE and GST-tagged full-length or cleaved CBS was respectively analyzed by the Monolith NT.115 (NanoTemper, Munich, Bavaria, DE). The Kd values for CBS and GE binding were computed using the mass action equation of the NanoTemper software.

2.15. Molecular docking

The binding sites between GE and CBS were analyzed using Discovery Studio 2019 based on the results of LiP-MS analysis. The protein X-ray crystal structure of the CBS model (PDB ID: 4COO) was downloaded from the RCSB Protein Data Bank database (http://www.rcsb.org/pdb). The small molecule was downloaded from PubChem (https://pubchem.ncbi.nlm.nih.gov/). Before the docking procedure, water molecules, solvent molecules, and ions were removed from CBS. Then CBS protein was cleaned and repaired, including the correction of non-standard amino acid names, the mending of incomplete residues, and the addition of hydrogens. Flexible docking was then performed with the screened LiP peptides defined as flexible residues and the regulatory domain active sites defined as a site sphere. The best-scoring docked model was finally selected to represent the most favorable binding mode.

2.16. Transmission electron microscope

After being injured by NaT or co-treated with GE for 1 h, isolated pancreatic acinar cells were quickly centrifuged and resuspended in a 0.5 % glutaraldehyde solution, allowing them to sit for 5 min at 4 °C. The cells were then fixed again with 2.5 % glutaraldehyde and 1 % osmium tetroxide. After completing the dehydration, permeabilization, and embedding processes, the cell samples were placed on a copper mesh using an ultrathin sectioning machine to create sections approximately 60–90 nm thick. Finally, the sections were stained in sequence with uranyl acetate and lead citrate, and then examined and photographed using a transmission electron microscope (HITACHI-HT7800, Tokyo, Japan).

2.17. Statistical analysis

All data were presented as mean ± standard error of the mean (SEM). Statistical analysis was performed using GraphPad Prism 9.0 software. Comparative analyses between two groups were conducted utilizing unpaired Student's t-test or Mann–Whitney test, while comparisons involving multiple groups were performed using One-Way ANOVA with Dunnett's multiple comparison tests or non-parametric tests with the Kruskal–Wallis H test. A significance level of $P < 0.05$ was established to denote statistical differences.

3. Results

3.1. GE reduced necrosis and oxidative stress in pancreatic acinar cells

GE is classified as a natural iridoid glycoside [12], and its chemical structure is shown in Fig. S1A. First, we examined the effect of GE on lactate dehydrogenase release from normal pancreatic acinar cells and found that GE exhibited no significant cytotoxicity under the concentrations of 25–100 μM (Fig. S1B). Next, we observed that GE at 50–100 μM showed protective effects on NaT-induced pancreatic acinar cell death, and the effect is optimal at a concentration of 75 or 100 μM (Fig. 1A–B). Based on the above results, 100 μM of GE was selected for subsequent cellular experiments. ROS generation is an important marker of oxidative stress in acinar cells. It is apparent that GE could significantly ameliorate ROS production induced by NaT (Fig. 1C–D, Fig.S2A) or H_2O_2 (Fig. S2B). GSH plays an important role in maintaining redox homeostasis. Interestingly, GSH in pancreatic acinar cells showed a dose-dependent depletion when stimulated by a concentration gradient of NaT (0.18, 1, 2, 4, and 6 mM) (Fig. S3A–B). While 100 μM of GE reversed the deficiency of cellular GSH under the stimulation of 4 mM NaT (Fig. 1E–F, Fig. S3C). Therefore, these results indicated that GE, especially at 100 μM suppressed oxidative stress and reduced pancreatic acinar cell necrosis.

3.2. GE ameliorated trypsinogen activation, oxidative stress, and pancreatic injury in CER-AP mouse models

Next, we further explored the pharmacological actions of GE on the experimental CER-AP mouse model. Firstly, we discovered that GE (14 mg/kg) simultaneously administered with the second CER injection (Fig. 2A) significantly ameliorated pancreatic pathological injury, including edema and inflammatory infiltration (Fig. 2B–C, Fig. S4A). The indicators related to trypsinogen activation, including pancreatic and serum trypsinogen activation peptide (TAP) (Fig. 2D–E) and pancreatic cathepsin B (CTSB) (Fig. S4B), were significantly elevated in AP mice and decreased following GE treatments. Consistent with this finding, pancreatic trypsin activity was remarkably decreased by GE (Fig. 2F). To observe inflammatory infiltration, the neutrophils in the pancreas were stained with MPO antibodies (Fig. 2G), accompanied by the biochemical measurement of MPO activity (Fig. 2H). As expected, there was more severe inflammation in the CER-AP group compared to the GE group. While GE showed no significant alterations in serum amylase and lipase (Fig. S4D), it pronouncedly restored pancreatic amylase expression *in situ* (Fig. S4C) [29]. Furthermore, pancreatic ROS overexpressed in CER-AP stained by BBoxiProbe-O13 was observed, while GE significantly reduced it (Fig. 2I). The ratio of GSH to GSSG can be used as a relative measure of oxidative stress [30], which was significantly decreased in serum and pancreas, and partly reversed by GE treatment (Fig. 2J). Meanwhile, GE at 14 mg/kg administered after the last injection of CER (Fig. S5A) also improved AP pathology, with pancreatic edema reaching significance (Fig. S5B–C). Pancreatic trypsin and MPO activities were evidently suppressed after GE treatment as the simultaneous treatment with GE, while serum amylase and lipase were reversed with a trend (Fig. S5D). Furthermore, the efficacy of GE on oxidative stress indicators in CER-AP models was investigated. It was demonstrated that GE obviously reduced pancreatic ROS production (Fig. S5E) and partially enhanced the activities of serum GPx (Fig. S5F) and SOD (Fig. S5G). In CER-AP, GSH accumulation in the pancreas was observed at 12 h, consistent with our previous findings [14]. After GE treatment, GSH upregulation was more pronounced (Fig. S5H). These results support the conclusion that GE could markedly inhibit the activation of trypsinogen to trypsin, restore redox homeostasis, and ameliorate pancreatic injury in CER-AP mouse models. And the earlier administration of GE resulted in more pronounced therapeutic efficacy.

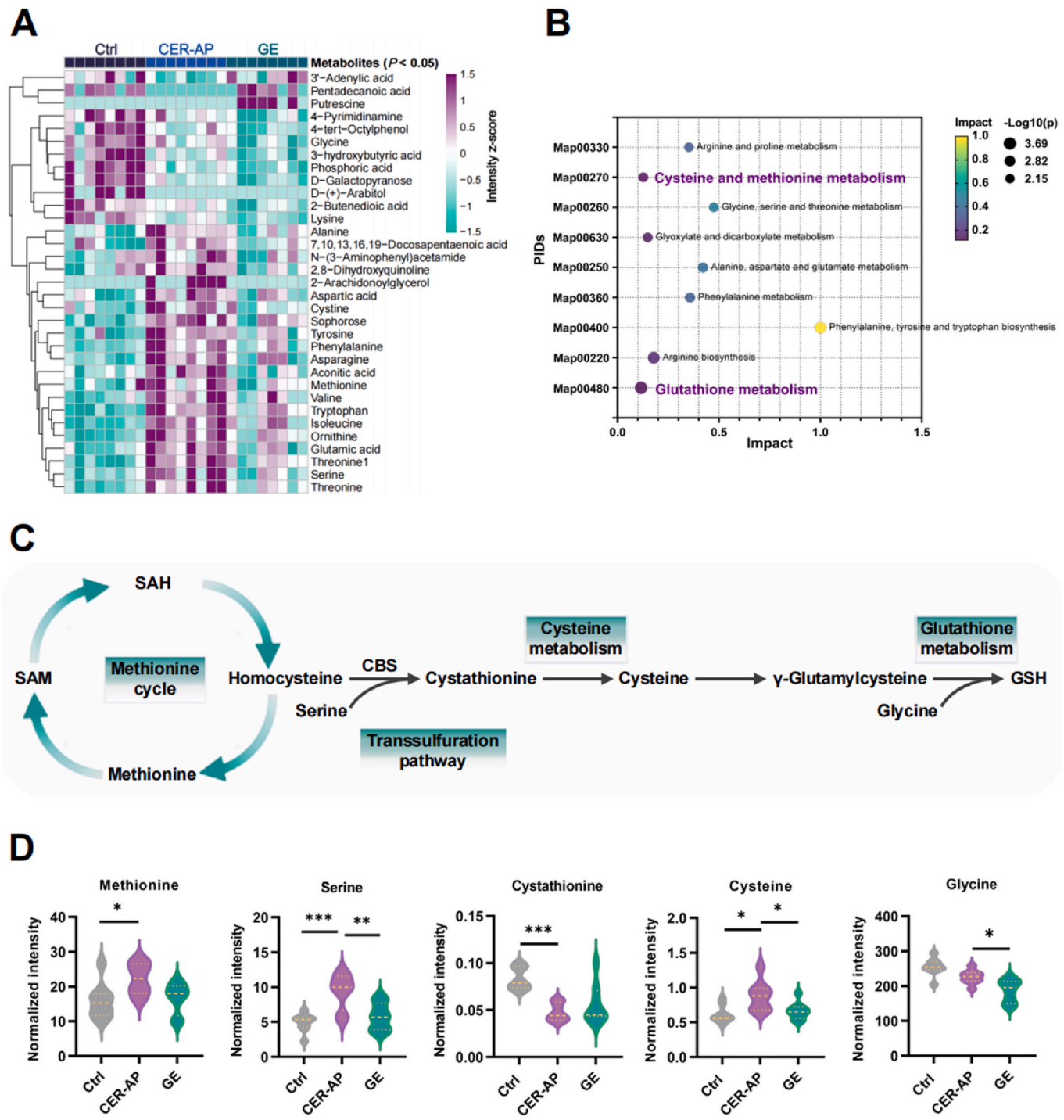

Fig. 3. GE restored cysteine and methionine metabolism in the pancreas of CER-AP mouse models. (A) Heatmap showing significantly altered metabolites in Ctrl, CER-AP, and GE groups ($n = 8$. $P < 0.05$). The color scale indicates low-intensity values in green and high-intensity values in purple. (B) The bubble diagram displays significantly interrupted metabolic pathways based on KEGG analysis. (C) An overview of the metabolic profiles for the methionine cycle, transsulfuration, and glutathione metabolism. (D) The violin plots showing changes in metabolites of cysteine and methionine metabolism as well as glutathione metabolism in three groups ($n = 8$). Data are presented as mean ± SEM; $^{*}P < 0.05$, $^{**}P < 0.01$, and $^{***}P < 0.001$.

3.3. GE restored cysteine and methionine metabolism in the pancreas of CER-AP mouse models

In order to explore the mechanism of GE improvement in AP, non-targeted metabolomic analysis was conducted to identify the characteristic metabolic profile in CER-AP. In total, 33 significantly differential metabolites ($P < 0.05$) were identified in the pancreas among Ctrl, CER-AP, and GE groups. As shown in the heatmap (Fig. 3A), these metabolites are primarily classified into three distinct clusters, with two of these clusters demonstrating significant readjustment. Further Kyoto Encyclopedia of Genes and Genomes enrichment (KEGG) analysis was performed based on these disturbed metabolites, and the top 9 enriched pathways are displayed in Fig. 3B. Among them, cysteine and methionine metabolism ($P = 0.0055$ and FDR = 0.0491) and GSH metabolism ($P = 0.0002$ and FDR = 0.0083) were significantly enriched, which caught our attention. A detailed analysis of metabolites in cysteine and

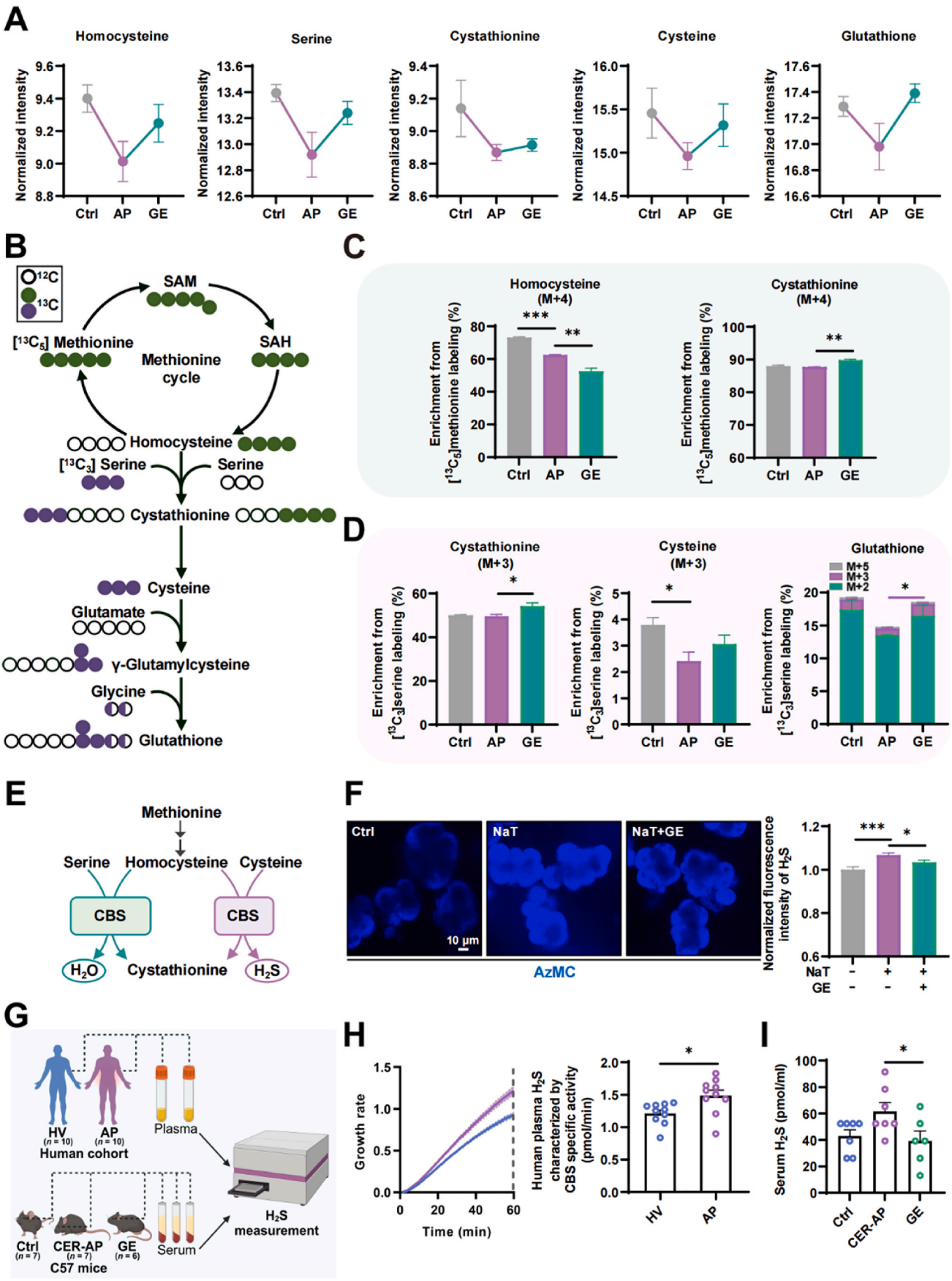

(caption on next page)

Fig. 4. GE reprogrammed the trans-sulfuration pathway, improved GSH synthesis, and reduced H_2S generation. (A) Targeted metabolites analysis for cysteine and methionine metabolism and GSH metabolism in pancreatic acinar cells from Ctrl, AP, and GE groups ($n = 3$). (B) The conceptual metabolism of [$^{13}C_5$]-methionine and [$^{13}C_3$]-serine tracing via the methionine cycle, transsulfuration, and GSH synthesis pathways. Green and purple cycles represent the isotopomers derived from [$^{13}C_5$]-methionine and [$^{13}C_3$]-serine, respectively. (C) The fractional contribution of [$^{13}C_5$]-methionine to homocysteine and cystathionine in acinar cells in three groups ($n = 3$). (D) The fraction labeling in cellular cystathionine, cysteine, and glutathione from [$^{13}C_3$]-serine in pancreatic acinar cells in three groups ($n = 3$). (E) A diagram showing CBS utilizes homocysteine together with different substrates, serine or cysteine, to produce H_2O or H_2S, respectively. (F) Fluorescence images showing the inhibition of GE (100 μM) on H_2S in NaT-induced pancreatic acinar cells by using a 7-azido-4-methylcoumarin (AzMC) probe, and their quantitative results of fluorescence intensity (normalized to Ctrl) on the right. H_2S could selectively reduce the aromatic azide component of AzMC, producing fluorescent 7-amino-4-methylcoumarin (AMC) which was detected at 450 nm. (Blue, AzMC. Bar = 10 μm. n = 18–23 cell clusters). (G) Schematic diagrams for circulative H_2S measurement in human plasma and murine serum. (H) Typical traces of H_2S generation characterized by CBS enzyme activity in human AP plasma and the quantitative analysis at 60 min ($n = 10$). (I) The effective role of GE (100 μM) in decreasing H_2S levels in the serum of CER-AP mice (n = 6–7). Data are presented as mean ± SEM; $^*P < 0.05$, $^{**}P < 0.01$, and $^{***}P < 0.001$.

methionine metabolism, as well as GSH metabolism, was performed (Fig. 3C). The relative abundance of methionine, serine, and cysteine was significantly elevated in AP groups, whereas the relative intensity of cystathionine and glycine was strikingly decreased in the model groups (Fig. 3D). GE returned the level of methionine, serine, cystathionine, and cysteine, with serine and cysteine reaching statistical significance. Taken together, GE affected cysteine and methionine metabolism in the pancreas of CER-AP, particularly exerting a remarkable alteration on the metabolites in the transsulfuration pathway.

3.4. GE reprogrammed the trans-sulfuration pathway, improved GSH synthesis, and reduced H_2S generation

To elucidate whether the metabolic regulation of *trans*-sulfuration by GE affects acinar cells, targeted metabolomics and metabolic flux analysis were respectively performed on freshly isolated pancreatic acinar cells. As shown in Fig. 4A, after stimulation with toxic NaT for 1 h, the intracellular metabolites were collected for targeted metabolomics analysis, and indicated that all the metabolites involved in the methionine cycle, cysteine metabolism, and GSH metabolism tended to decrease in the AP group and were restored by GE treatment. Next, the labeled ratio of metabolites in these pathways from [$^{13}C_5$]-methionine and [$^{13}C_3$]-serine in pancreatic acinar cells was traced, respectively (Fig. 4B). Firstly, by tracing [$^{13}C_5$]-methionine into downstream intermediates and metabolites, the carbon atoms are directly incorporated into homocysteine and cystathionine, and the enrichment ratio of M+4 for homocysteine was down-regulated in the AP group and further decreased in the GE group (Fig. 4C). In contrast, the enrichment ratio of M+4 for cystathionine was only up-regulated in the GE group (Fig. 4C). When tracing [$^{13}C_3$]-serine, a higher enrichment of cystathionine [M+3] was also observed in the GE group (Fig. 4D). Additionally, GE improved the enrichment of cysteine [M+3] and GSH [M+3] (Fig. 4D). These data indicated that GE activated the *trans*-sulfuration pathway and enhanced GSH synthesis in injured acinar cells.

As the first rate-limiting enzyme in the *trans*-sulfuration pathway, CBS has an independent role not only as a homocysteine-metabolizing enzyme using serine as a substrate, but also as an enzyme utilizing homocysteine and cysteine to produce H_2S under the physiological conditions (Fig. 4E) [31]. Consequently, we aim to explore whether the production of H_2S is likewise activated by GE. *In vitro*, various concentrations of NaT (4, 6, and 9 mM) significantly increased CBS enzyme activity for H_2S detection in cell supernatant compared with the untreated group (Fig. S6A). Furthermore, GE reduced the buildup of H_2S induced by 9 mM NaT (Fig. S6B). Presented by H_2S staining with the 7-azido-4-methylcoumarin probe, H_2S generation in pancreatic acinar cells was elevated in the NaT-induced group while reversed in the GE group (Fig. 4F, Fig. S6C). We also examined the peripheral CBS activity (Fig. 4G), and increased H_2S was found in both AP patients (Fig. 4H) and AP mice (Fig. 4I). GE significantly inhibited H_2S production in serum (Fig. 4I). Above all, those results collectively suggest that GE activated CBS in *trans*-sulfuration metabolism for GSH synthesis instead of CBS for H_2S production.

3.5. GE had a weak interaction with CBS but did not directly regulate CBS enzymatic activity

Then, we aimed to investigate whether there is a direct interaction or regulatory relationship between GE and CBS. The microscale thermophoresis analysis suggested that the full-length CBS bound to GE with a K_D estimated at 38.38 μM (Fig. 5A). Meanwhile, the cellular thermal shift assay was performed to investigate the stability of CBS in pancreatic acinar cells under NaT exposure. As expected, GE (100 μM) increased the thermal stability of CBS in pancreatic acinar cells, while rising temperatures reached statistical significance only at 68 °C (Fig. 5B–C, Fig. S7). To further elucidate GE-CBS interactions and the associated conformational changes, LiP-MS analysis on full-length CBS in the presence and absence of GE was performed (Fig. 5D). Recombinant CBS was subjected to limited proteolysis using a non-specific protease under controlled conditions, leading to measurable shifts in the abundance of proteolytically derived peptide fragments (Fig. 5D). The resulting peptide fragments were then analyzed by mass spectrometry, showing 425 shared peptides in the Ctrl and GE groups and 3 down-regulated LiP peptides with statistical significance ($|\log_2 FC| > 1.5$ and $P < 0.05$) after GE treatment (Fig. 5E). Two altered peptides were detected in the regulatory domain, and one was partly in the catalytic domain upon the addition of GE (Fig. 5E). Further flexible docking by computer simulation revealed that GE formed hydrogen bonds with full-length CBS via Gly418, Ser 420, and Gln445 and formed Pi-alkyl interaction with Leu417, Leu419, Leu499, Val534, and Leu539 (Fig. 5F), which suggested that GE interacted with CBS primarily in the regulatory domain and triggered corresponding conformational changes. Remarkably, the microscale thermophoresis analysis indicated that the cleaved CBS variant had reduced binding affinity for GE compared to the full-length protein (Fig. S8A), further validating the above finding. Accordingly, GE weakly bound to CBS through allosteric binding.

To deeply explore the regulation of GE on CBS enzyme activity, SAM, a well-known allosteric activator mainly acting on the regulatory domain of full-length CBS, was included as a positive control. The prominently increased enzyme activity on H_2S generation with cysteine and homocysteine as substrates was detected in the SAM group but not in the GE group (Fig. S8B). Consistently, the simultaneously generated cystathionine (unlabeled) was not significantly changed upon the addition of GE (Fig. 5G–H). Meanwhile, the enrichment ratio of cystathionine [M+3] was also not altered (Fig. 5I) with [$^{13}C_3$]-serine added into the enzymatic reaction system of full-length CBS (Fig. 5G), suggesting GE did not directly affect CBS enzyme activity. There were similarly no significant impacts of GE on the enzyme activity for cleaved CBS (Fig. S8C). Thus, GE had an extremely weak interaction with CBS and could even cause limitations on the direct regulation of CBS enzymatic activity and pharmacological CBS targeting, further implying the primary regulatory mechanism of GE might be indirect.

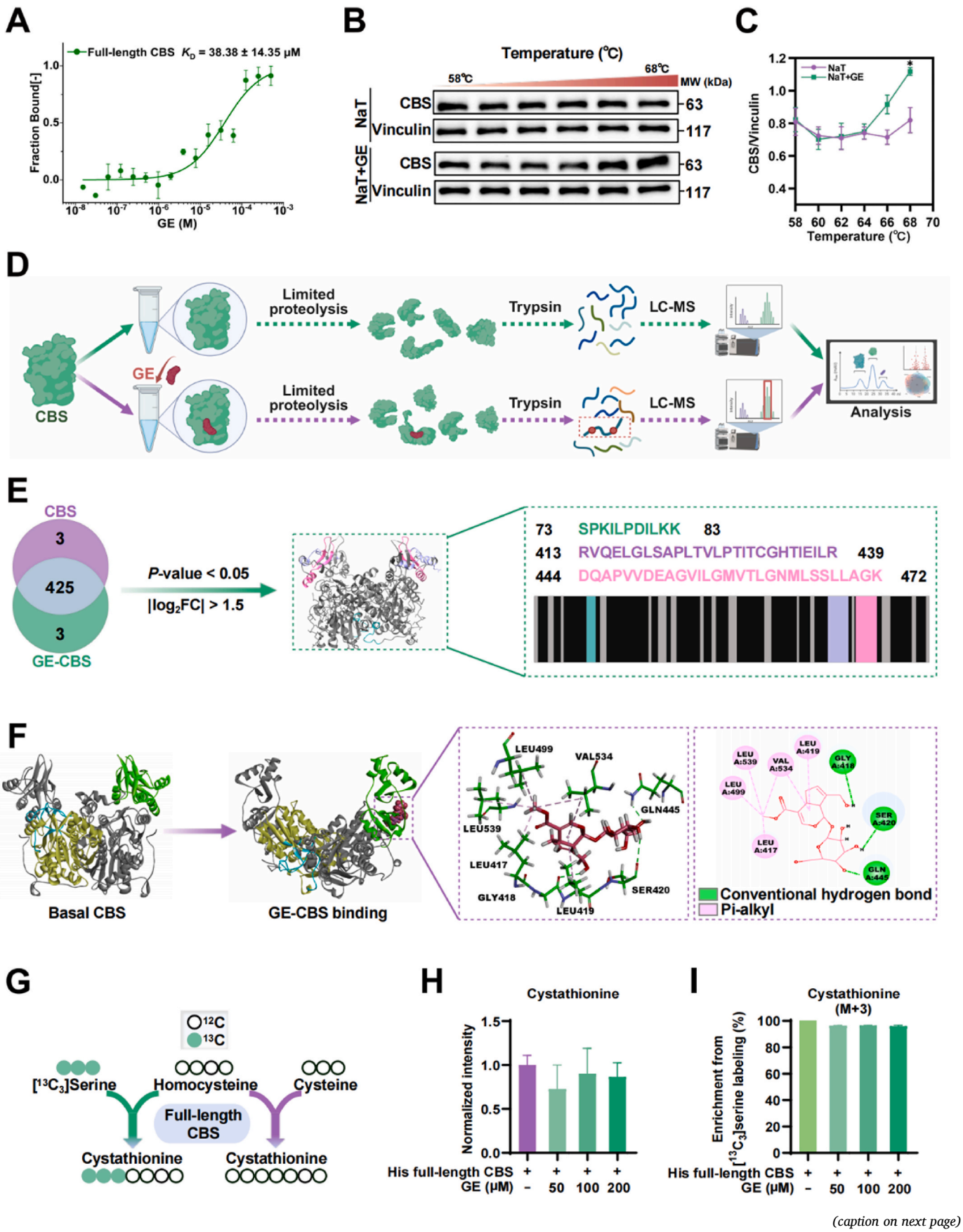

(caption on next page)

Fig. 5. GE had a weak interaction with CBS but did not directly regulate CBS enzymatic activity. (A) Microscale thermophoresis analysis showing the interaction of GE with recombinant full-length CBS. (B) Cellular thermal shift assay showing GE treatment increased the thermal stability of CBS in NaT-induced acinar cells across a narrow temperature range, with statistical significance only at 68 °C. (C) Summary quantification results for CBS protein expressions in NaT-induced pancreatic acinar cells at ranges of 58–68 °C ($n = 3$). (D) Flow chart depicting the LiP-MS analysis for full-length CBS in the presence and absence of GE. The CBS protein with different treatments was subjected to limited proteolysis by proteinase K in the native condition, followed by trypsin digestion and mass spectrometry detection of peptide abundance. (E) Conformational alterations in CBS induced by GE incorporation. Venn diagrams indicating the number of peptides detected in the GE and Ctrl groups. Significant CBS LiP peptides ($|\log_2 FC| > 1.5$, $P < 0.05$) mapped to the 3D structure (PDB: 4COO) revealed purple and deep rose peptides localized in the regulatory domain, while green peptides partially occupied the catalytic domain. The structural barcode visually displayed the peptide distribution mapped along the CBS sequence from N- to C-terminus, where black and gray bars respectively represented detectable peptides without significant abundance changes and undetected peptides after GE treatment, while green, purple, and deep rose regions marked sequence-specific peptides with significant alterations. (F) Flexible docking of GE (red) binding to CBS and detailed protein-ligand complex interactions. GE-CBS binding indicating structural changes for basal CBS and showing Leu417, Gly418, Leu419, Ser420, Gln445, Leu499, Val534, and Leu539 as binding sites. The regulatory and catalytic domains of CBS were respectively colored green and yellow, with blue loops (L145–148, L171–174, L191–202, and L295–316) marking the active site entrances. (G) Scheme of full-length CBS activity profiling through cystathionine production from distinct substrate sources. In the presence of cysteine and homocysteine, CBS catalyzed unlabeled cystathionine generation, whereas high-concentration [$^{13}C_3$]-serine tracing shifted the product profile predominantly to [M+3] cystathionine. Green circles denoted isotopomers derived from [$^{13}C_3$]-serine. (H) CBS enzyme activity was characterized by the intensity of unlabeled cystathionine ($n = 3$–4). (I) The enzyme activity assay for detecting fractional contributions of [$^{13}C_3$]-serine to cystathionine [M+3] ($n = 3$–4). Vinculin serves as a loading control for immunoblots. Data are presented as mean ± SEM; $^*P < 0.05$.

3.6. GE reduced the production of the CBS truncated form that was primarily responsible for the enhanced enzymatic activity on H_2S generation

Next, we sought to investigate whether GE modulated enzymatic activity by influencing the protein expression or post-translational modifications of CBS. Due to the blockade of transsulfuration in the CER-AP [7], the pancreatic protein expression and mRNA levels of CBS were significantly decreased at the inflammatory peak in the AP group according to our previous time-course CER-AP model [14] (Fig. S9). In line with the aforementioned results, a marked reduction was observed in the *Cbs* mRNA level at 12 h (Fig. 6A), while the protein expression presented a decreasing tendency in the AP group (Fig. 6B–C). Nevertheless, GE exerted no effect on the transcriptional level of CBS (Fig. 6A) but significantly augmented the protein expression (Full-length, 63 kDa) (Fig. 6B–C). It is noteworthy that the expression of cleaved CBS protein (approximately 48 kDa) was significantly enhanced on average in the AP group, though variable between animals, and was mitigated following GE administration (Fig. 6B–C). These results indicated that GE affected the post-translational modification of CBS by reducing the generation of its truncated variants. Consistent with the *in vivo* finding, the expression of full-length CBS was significantly lessened in a concentration-dependent manner in NaT-induced pancreatic acinar cells at concentrations of 4, 6, and 9 mM (Fig. S10). Meanwhile, GE showed an improvement in full-length CBS and a reduction in cleaved CBS of acinar cells under 4 mM-NaT stimulation (Fig. 6D–E). Overall, CBS protein probably underwent proteolytic degradation, a protein post-translational modification in pancreatic acinar cells during AP, which was rescued by GE.

Since trypsin could hydrolyze full-length CBS, the possible major hydrolysis sites, including Lys 36 and Arg 413, were shown in Fig. 6F [25]. Previous studies revealed that the full-length CBS could be hydrolyzed with trypsin at the Arg 413 residue, resulting in an active, cleaved monomer (about 48 kDa) production [25,32]. To understand whether the cleaved CBS is optimal for H_2S generation, we continuously performed recombinant protein expressions of the two kinds of CBS and monitored their enzyme activity on H_2S generation. Consistent with prior data [33], the enzyme activity of cleaved His-CBS was higher than full-length His-CBS (Fig. 6G). SDS-PAGE revealed distinct bands corresponding to the two proteins (Fig. 6H). Then, we simulated the pathological process of trypsin activation and subsequent hydrolysis of CBS within acinar cells *in vivo* during AP by treating the full-length CBS protein with trypsin. When co-incubating His-CBS with various concentrations of trypsin (1, 5, 10, and 20 nM, respectively), the enzymatic activity of full-length His-CBS tended to increase, especially at 10 nM (Fig. 6I). Simultaneously, multiple hydrolysis bands were observed on the SDS-PAGE gel after trypsin intervention. Notably, the bands about 48 kDa became more intense after treatment with 10 nM trypsin (Fig. 6J). In addition, co-incubating 100 nM trypsin with full-length GST-CBS also demonstrated a significant elevation in enzymatic activity (Fig. S11A). Furthermore, prior to trypsin processing, we added GE (200 and 400 μM, respectively) to the full-length His-CBS. It was obvious that an increase without statistical significance of CBS enzyme activity was observed in the GE group (Fig. S11B), and GE did not stabilize the full-length CBS from trypsin-mediated proteolysis, as presented by SDS-PAGE (Fig. S11C). Therefore, GE did not prevent CBS from trypsinolysis through their pre-interaction, and it has no direct impact on the enzyme activity of the cleaved variant (Fig. S8C). Alternatively, prior to full-length CBS addition, pre-incubating GE (200 and 400 μM) with trypsin inhibited the activity of proteolytic CBS (Fig. S11D). Taken together, these findings indicate that the CBS truncation of H_2S generation, mainly mediated by trypsin, is a critical post-translational modification in AP states. However, this modification and its resulting elevated truncation activity cannot be directly inhibited by GE-CBS interaction, likely due to the indirect mechanism of GE acting on trypsin.

3.7. GE inhibited trypsinogen activation

It is well-known that premature intracellular activation of trypsin is the most important pathological event. Based on the inhibition of pancreatic trypsin in CER-AP mouse models (Fig. 2D–F, Fig. S4B, Fig. S5D), we further explored the effect of GE on trypsinogen activation in pancreatic acinar cells *in vitro*. Firstly, we detected that the specific TAP, a parameter indicating trypsinogen activation, showed significant enhancement in NaT-induced acinar cells, with GE treatment exhibiting greater suppression than the positive controls (Fig. 7A–B, Fig. S12A). Then, zymogen granules in freshly isolated pancreatic acinar cells were analyzed under transmission electron microscopy. The number of zymogen granules (per cell) just tended to decrease after NaT-induced for 1 h and increased by GE treatment (Fig. 7C). Accordingly, the elevated trypsin activity in NaT- (Fig. 7D) or CER-stimulated (Fig. S12B) pancreatic acinar cells was able to be downregulated by GE, similar to the positive trypsin inhibitors (Fig. S12C). And the BZiPAR fluorescent probe for detecting trypsin activity further confirmed the effects of GE (Fig. 7E–F). These findings collectively indicate that GE plays a critical role in inhibiting trypsinogen activation in pancreatic acinar cells, thereby reducing trypsin-mediated degradation of full-length CBS. The resulting reprogramming of the transsulfuration metabolism, achieved by the decreased post-translational modification of truncated CBS, enhances GSH synthesis while decreasing H_2S production, ultimately protecting against AP (Fig. 8).

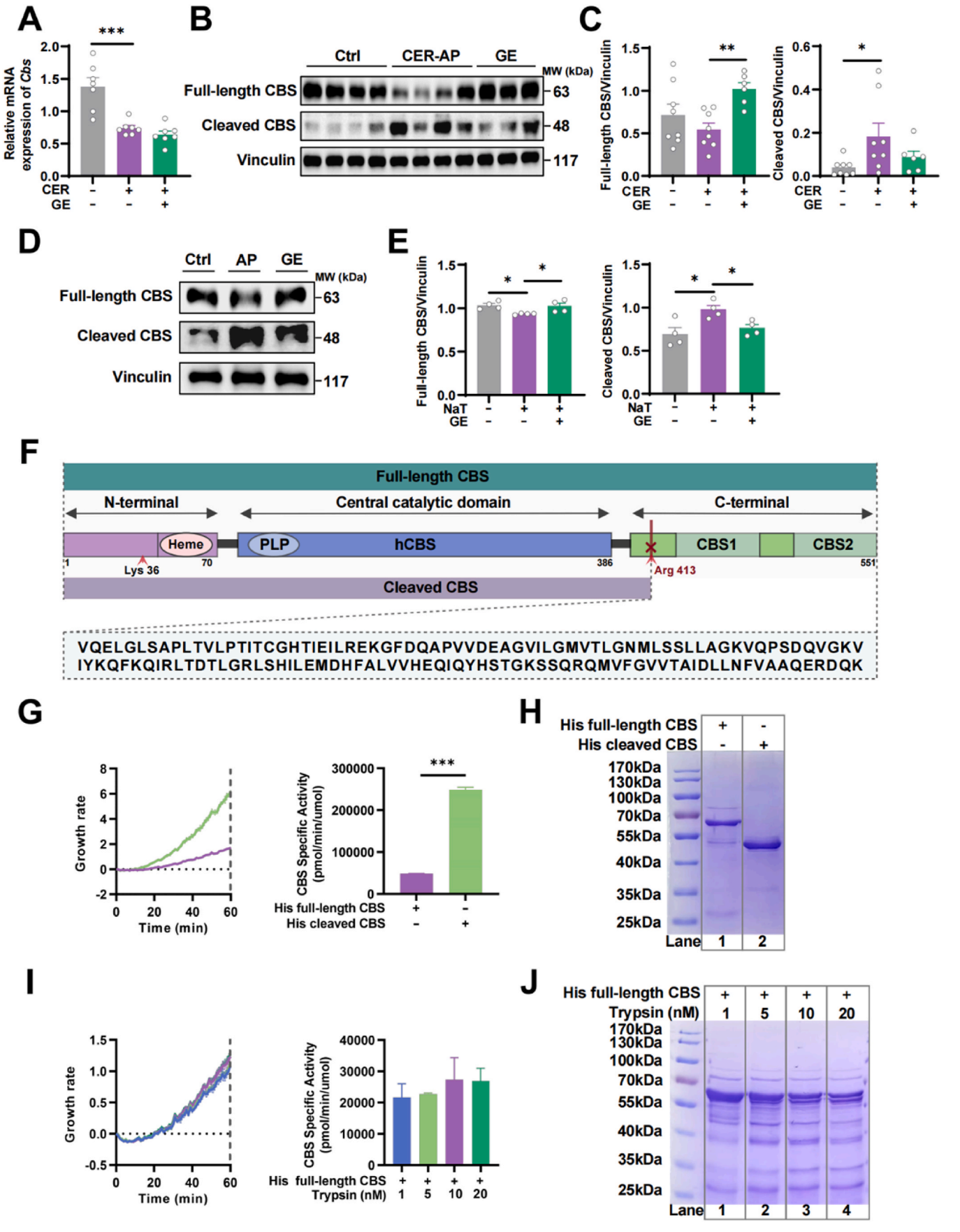

(caption on next page)

Fig. 6. GE reduced the production of the CBS truncated form that was primarily responsible for the enhanced enzymatic activity on H_2S generation. (A) Pancreatic mRNA expression of *Cbs* in CER-AP mouse models ($n = 7$). (B) WB images of full-length and cleaved CBS protein expression in the pancreas of CER-AP mouse models. (C) Quantitative analysis for full-length and cleaved CBS proteins in the pancreas from three groups ($n = 6$–8). (D) WB analysis of full-length and cleaved CBS expression in pancreatic acinar cells stimulated by NaT and treated with GE (100 μM). (E) Quantitative results of full-length and cleaved CBS expression in pancreatic acinar cells from three groups ($n = 4$). (F) Schematic representation of the structure for full-length and cleaved CBS with the major sites where full-length CBS may be hydrolyzed by trypsin. (G) The enzyme activity was monitored for H_2S generation of full-length and cleaved CBS ($n = 3$). (H) SDS-PAGE analysis of purified recombinant full-length and cleaved CBS protein blots after eStain L1 staining. (I) The enzymatic activity was monitored for H_2S generation of full-length CBS proteins after hydrolysis by trypsin (1, 5, 10, and 20 nM) ($n = 3$). (J) SDS-PAGE analysis of purified recombinant full-length CBS hydrolyzed by various concentrations of trypsin after eStain L1 staining. Vinculin serves as a loading control for immunoblots. Data are presented as mean ± SEM; $^*P < 0.05$, $^{**}P < 0.01$, and $^{***}P < 0.001$.

4. Discussion

Metabolic mechanisms play a crucial role in maintaining homeostasis, which collectively ensures energy production and utilization as well as redox balance [34]. Dysregulation of these metabolic pathways can lead to metabolic disorders and aggravate various diseases, including AP [4]. AP is an inflammatory condition of the pancreas characterized by the premature activation of digestive enzymes within the pancreatic acinar cells, leading to autodigestion and pancreatic damage [2]. This results in the release of pro-inflammatory cytokines, recruitment of immune cells, and systemic inflammatory response, potentially leading to complications such as pancreatic necrosis and multi-organ failure [2,35]. Understanding the interplay among metabolic dysregulation, premature activation of trypsinogen, and inflammation is essential for developing targeted therapies for preventing disease progression in early AP. Here, we have provided convincing evidence suggesting that GE could inhibit trypsinogen activation on AP models both *in vivo* and *in vitro*. This suppression ultimately results in diminished proteolytic modification of CBS, thereby reprogramming the transsulfuration pathway, enhancing GSH synthesis, and reducing inflammatory H_2S production. This is the first report regarding the association of metabolic dysfunction with the core pathogenesis of AP, the activation of trypsinogen and oxidative stress. It emphasizes the importance of regulating the metabolic enzyme CBS and metabolic flux as well as identifies a novel target for disease therapy. Meanwhile, this study offers a natural leading drug, geniposide, capable of inhibiting the early activation of trypsinogen and potentially regulating the post-translational modifications and biological processes of various proteins.

GE, a prominent iridoid glycoside isolated from *Gardenia jasminoides J. Ellis*, has garnered significant attention for its potent anti-inflammatory and antioxidant effects, which make it a promising therapeutic agent for various inflammatory diseases, such as rheumatoid arthritis, inflammatory bowel disease, neurodegenerative disorders, and liver injury [12]. Several studies have indicated that GE may exert protective effects on acinar cells. For instance, Zhang et al. previously reported that GE can attenuate LPS-induced cellular damage in AR42J cell lines [36]. While the aglycone of geniposide, geniposidic acid, has been shown to possess lipase inhibitory activity [12]. However, the direct therapeutic efficacy of GE in treating AP remains to be further verified. In this study, we demonstrated that GE, particularly at a concentration of 100 μM, protected primary pancreatic acinar cells from oxidative stress and necrosis. Since oral GE exhibited higher hepatotoxicity and lower bioavailability owing to enterohepatic recirculation, whereas the favorable aqueous solubility of GE makes it suitable for intravenous delivery in early fasting AP [12], tail vein injection was finally selected for *in vivo* studies. GE at 14 mg/kg inhibited the activation of trypsinogen and MPO, improved oxidative stress, and alleviated pancreatic edema and inflammation in CER-AP. These findings together confirm that GE is the major active component in both *Gardenia jasminoides J. Ellis* and Chaiqin Chengqi decoction, contributing to their *anti*-AP effects.

Methionine metabolism through the *trans*-sulfuration pathway decisively contributes to the maintenance of redox homeostasis in cells [37]. As the two most significant metabolites downstream of the transsulfuration pathway, cysteine and GSH, are both capable of exerting therapeutic efficacy on AP at an early stage, and this is associated with their antioxidant functions [6,38]. The current study confirmed that both cysteine and GSH were decreased in NaT-induced pancreatic acinar cells by targeted metabolomics analysis and flux analysis. While GE restored the concentrations and the flux of these two metabolites, and improved the GSH synthesis. GSH is a tripeptide composed of three amino acids: glutamate, cysteine, and glycine [39]. Among these, cysteine is the rate-limiting precursor because its availability often determines the overall rate of GSH synthesis [40]. In the context of the *trans*-sulfuration pathway, cysteine is synthesized from homocysteine via cystathionine as an intermediate [41]. Therefore, the regulation of *trans*-sulfuration is crucial for maintaining cellular redox homeostasis, and GE plays an important role in this part.

CBS is the gatekeeper of the *trans*-sulfuration pathway, controlling the flow of metabolites (homocysteine, cystathionine, and cysteine) and influencing GSH synthesis and H_2S production [42]. It was formerly postulated that the obstruction of transsulfuration and the suppression of CBS enzymatic activity exacerbated AP [7], yet the underlying cause remained elusive. However, allosteric activation of CBS by SAM did not alleviate but aggravated AP [7]. The enzymatic activity is also regulated by the substrate except for SAM. Typically, the affinity of CBS for serine is 7–10 times than that for cysteine, and therefore is more prone to generate H_2O rather than H_2S [9]. In AP, H_2S can enhance the release of substance P from sensory nerves, mainly amplifying inflammation and pain [8,43]. Here, a reduced level of serine, cysteine, and GSH was first observed in NaT-stimulated pancreatic acinar cells, while an overproduction of H_2S was also found. Notably, GE is capable of reversing the metabolic flux, including enhancing GSH production and reducing H_2S generation, when decreasing CBS enzyme activity. Given that reduced GSH in the pancreas and oxidative stress are key features in the early course and severe progression of AP [6,37], we speculate that rapid GSH restoration may be more critical for therapeutic efficacy in early-stage AP, while H_2S reduction may be more beneficial in the inflammatory amplification stage. Next, we intended to further explore whether this regulatory effect on CBS is direct or indirect. Firstly, we validated that GE weakly bound to CBS via microscale thermophoresis analysis and cellular thermal shift assay. In fact, the affinity is likely too weak to be pharmacologically relevant *in vivo* for direct CBS targeting. Then, the applied LiP-MS demonstrated GE-CBS binding primarily modified 2 proteolytic peptides in the regulatory region of CBS while minimally impacting the catalytic domain. Flexible docking similarly positioned the interaction site within the regulatory domain, further proving the CBS conformational changes. To assess whether the structural change affected CBS enzyme activity, the canonical allosteric activator SAM was chosen as a positive control. While SAM markedly stimulated full-length CBS activity, GE showed no effect, which might connect the previous finding that SAM exacerbated AP to H_2S overproduction [7]. Comparative studies of SAM-CBS and GE-CBS binding showed that GE mainly had allosteric interaction with the CBS regulatory domain but without the pronounced active-site exposure characteristics of SAM, consistent with their distinct effects on enzymatic activities [44]. Moreover, unchanged enrichment ratio of cystathionine [M+3] from [$^{13}C_3$]-serine and unlabeled cystathionine from cysteine revealed that GE regulates CBS enzyme activity without substrate

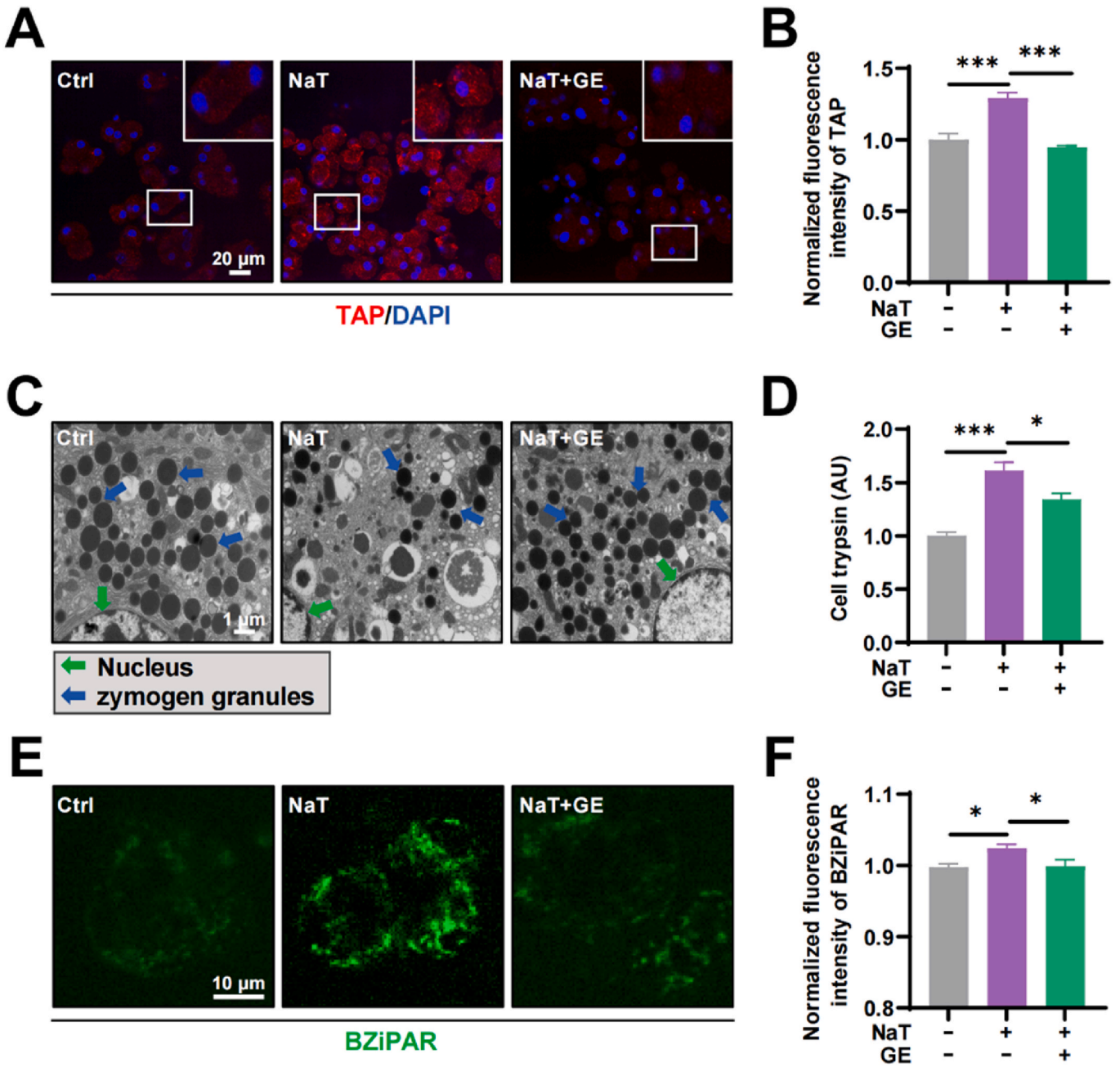

Fig. 7. GE inhibited trypsinogen activation in pancreatic acinar cells. (A) Representative immunofluorescence images of TAP expression for GE intervention under NaT stimulation in pancreatic acinar cells. TAP is the cleavage fragment released during the conversion of trypsinogen to trypsin (Blue, DAPI; red, TAP. Bar = 20 μm). (B) The quantification for fluorescence intensity (normalized to Ctrl) on positive TAP expressions in acinar cells (n = 4 ROIs). (C) Transmission electron microscopy images showing abundance of zymogen granules in pancreatic acinar cells in three groups (Green arrows, nucleus; blue arrows, zymogen granules. Bar = 1 μm). (D) Trypsin activity of pancreatic acinar cells was analyzed at 1 h under the stimulation by NaT and treatment by GE (100 μM) (n = 3). (E) Representative confocal microscopy images showing the trypsin activity by using the BZiPAR probe in acinar cells. BZiPAR was a substrate for trypsin and emitted green fluorescence when cleaved by trypsin (Green, BZiPAR. Bar = 10 μm). (F) The quantitative results of BZiPAR fluorescence intensity (normalized to Ctrl) (n = 11 cell clusters). Data are presented as mean ± SEM; $^{*}P < 0.05$ and $^{***}P < 0.001$.

selectivity. Accordingly, GE had a weak interaction with the regulatory domain of CBS but did not directly regulate CBS enzymatic activity.

Notably, the enzymatic activity of CBS might be significantly influenced by its post-translational modifications, with the most pronounced effect observed in the proteolytically truncated CBS [9,45]. In contrast to the other post-translational modifications, the degraded CBS has a conserved active core which has a higher specific activity than the normal form of CBS and is no longer regulated by SAM [25,46]. In this study, we have identified the presence of truncated CBS in the AP group and approved that the enzyme activity for H_2S production of truncated CBS is higher than that of full-length CBS. Hence, the cleaved CBS leads to metabolic reprogramming in the *trans*-sulfuration pathway, with the metabolic flux being more inclined to utilize cysteine for generating H_2S rather than serine for generating H_2O. This is aligned with our previous investigation of a marked reduction of serine and a decreased protein expression of full-length CBS, while an elevated cystathionine on a time-course AP model [14]. CBS is subjected to degradation by various proteases, and the specific lower-molecular-weight form of CBS with high activity could be recreated *in vitro* by trypsin incubation, but without other confirmed pancreatic proteases [9,25,47]. Since

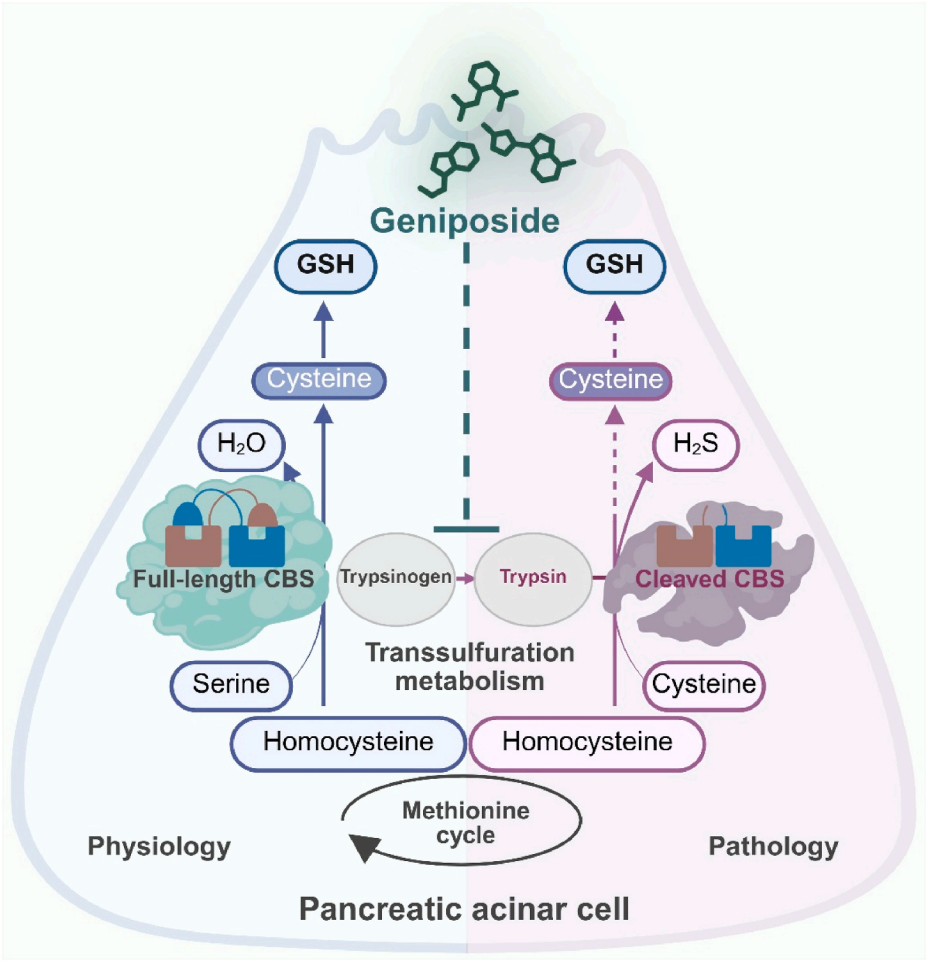

Fig. 8. GE reprogrammed transsulfuration metabolic flux in AP via inhibiting trypsinogen activation-mediated post-translational modification. Physiologically, trypsinogen in pancreatic acinar cells mainly remains inactive, with full-length CBS regulating normal transsulfuration metabolism via the initial catalysis of serine and homocysteine. However, the abnormal activation of trypsinogen to trypsin could increase the proteolytic post-translational modification of the full-length CBS in AP. By utilizing cysteine and homocysteine, the cleaved CBS boosted H_2S production and altered metabolic flow in the *trans*-sulfuration metabolism. GE could inhibit trypsinogen activation to prevent the post-translational modification for degrading full-length CBS and generating truncated variants both *in vitro* and *in vivo*. Therefore, stabilized full-length CBS would reincrease the utilization of serine and homocysteine, resulting in normal *trans*-sulfuration metabolic flux and promoting GSH generation. Image created in https://BioRender.com.

chymotrypsin could protect the pancreas by degrading trypsin [48], we added a specific chymotrypsin inhibitor TPCK when validating trypsinolysis on recombinant CBS [25]. Accordingly, we observed that the increasing concentrations of trypsin led to CBS degradation identical to pancreatic CBS profiles in AP models and reported studies [25], accompanied by a trend of elevated enzyme activity, suggesting a critical role of trypsin in the CBS post-translational modifications. Furthermore, we explored whether the reduction of cleaved CBS under GE conditions might result from the direct GE-CBS binding that pre-stabilizes CBS. Nevertheless, the pre-incubation of GE and recombinant CBS protein failed to diminish the degradation of full-length CBS by trypsin. Markedly, the inhibited activity of proteolyzing CBS was observed during the pre-incubation of GE and trypsin, firmly proving the target effects of GE on trypsin but not other proteases. The above-mentioned results further suggest that the stabilization of full-length CBS by GE is indirect.

Premature trypsinogen activation, in turn, initiates pancreatic autodigestion and induces the damage and death of acinar cells, triggering cytokine storms is a key pathological event in AP [2,35,49]. Trypsinogen, the inactive precursor of trypsin, is always stored in zymogen granules within pancreatic acinar cells [48,49]. The zymogen granules are synthesized through the trans-Golgi network and mature during transportation toward the apical region by the intracellular vesicle transport machinery, ultimately being released into the intestine for activation and physiological function [50]. Pancreatic secretory trypsin inhibitor, the rising pH in zymogen granules, and compartmentalization can prevent premature activation in the pancreas [51]. However, harmful stimuli during apical secretion could enhance the basal exocytosis and membrane disruption of zymogen granules, thereby accelerating AP [52,53]. Specifically, cathepsin B activates trypsinogen formed by co-localization of zymogen and lysosomes, and subsequently active trypsin enhances the permeability of these organelles, leading to organellar content leakage into the cytosol and acinar cell death in AP [2,54]. This process might induce progressive depletion of zymogen granules, a finding consistent with our electron microscopy results [53]. Previous studies have established that GE-derived *Gardenia jasminoides J. Ellis* extract stabilizes membrane structures to inhibit lysosomal enzyme leakage [55]. Consistently, GE tended to reduce CTSB expression in the pancreas tissues of CER-AP mice. Our *in vitro* and *in vivo* measurements proved GE markedly reduced TAP, a specific cleavage product released during trypsinogen conversion to trypsin, showing stronger suppression in acinar cells than the positive trypsin inhibitors SBTI and aprotinin. These findings confirmed the unique role of GE in inhibiting trypsinogen activation. As evidenced by both BZiPAR probe tracing and enzymatic activity assays, GE was found to suppress trypsin activity. Overall, these results collectively proved that GE markedly

inhibits the activation of trypsinogen into trypsin, which substantiated the properties of *Gardenia jasminoides J. Ellis* for modulating pancreatic enzyme secretion [55]. Furthermore, upon further discovery from recombinant protein studies, GE regulates the CBS post-translational modification of proteolytic cleavage at least via its impact on direct trypsin inhibition. Additionally, abnormally activated trypsin induces oxidative stress and depletes GSH [56,57], consistent with our findings of reduced GSH and altered GSH/GSSG ratios due to metabolic reprogramming. This further highlights the crosstalk between pathological mechanisms of AP and metabolic processes.

Among natural products with therapeutic potential against AP, GE offers distinct advantages. It is a key component of classical *anti*-AP formulas [58] and exhibits core anti-inflammatory and antioxidant activities. Crucially, GE uniquely inhibits upstream trypsinogen activation, a mechanism distinct from downstream-targeting natural compounds [59]. Furthermore, it is a non-peptide small molecule protease inhibitor and has more advantages compared with other peptide or protein drugs that lack selectivity and have short half-lives [60,61]. Therefore, GE serves as a valuable lead compound for developing trypsin inhibitors or optimized CBS activators.

In fact, the generation of H_2S is highly complex and can be catalyzed by both CBS and Cystathionine γ-lyase (CSE) from similar substrates [62]. The precise biological functions of CSE in terms of cysteine or H_2S production remain to be fully elucidated. In our study, we found decreased CSE protein expressions in the AP group, and GE showed no significant effect on either mRNA or protein expressions of CSE (Fig. S13). Due to the challenges associated with gene knockout in short-lived primary acinar cells *in vitro*, further studies involving recombinant protein expression and metabolic flux analysis using various isotopically labeled substrates may be required to confirm the role of CSE in AP and its potential regulation by GE through post-translational modifications.

5. Conclusion

In conclusion, the early abnormal activation of trypsinogen results in proteolytic CBS. This cleaved CBS promotes metabolic reprogramming of the transsulfuration pathway, generating fewer beneficial molecules like cysteine and GSH, while producing more inflammatory mediators such as H_2S, thereby intensifying oxidative stress and inflammation. As geniposide is capable of inhibiting the premature activation of trypsinogen both *in vivo* and *in vitro*, it can prevent this metabolic reprogramming and the aggravation of pathological events, thereby protecting against AP. This study, for the first time, explored the regulatory mechanism of natural products on the interplay among metabolic disorders, abnormal activation of trypsinogen, oxidative stress, and inflammation, revealing the characteristics of small molecules in multi-pathway intervention and further clarifying the advantages of traditional Chinese medicine or compound formulas in the treatment of complex diseases.

CRediT authorship contribution statement

Ji Gao: Writing – original draft, Visualization, Validation, Formal analysis, Data curation. **Yijing Long:** Writing – original draft, Visualization, Formal analysis. **Jiawang Li:** Validation, Investigation, Data curation. **Yiqin Wang:** Validation, Investigation, Data curation. **Rui Wang:** Validation, Investigation. **Jinxi Yang:** Validation, Data curation. **Jie Zhang:** Validation, Investigation. **Chenxia Han:** Investigation, Funding acquisition. **Qing Xia:** Supervision, Funding acquisition, Conceptualization. **Dan Du:** Writing – review & editing, Supervision, Funding acquisition, Conceptualization.

Declaration of competing interest

The authors declare no conflicts of interest. Signed by all authors as follows:

Acknowledgments

We acknowledged the funding from the National Natural Science Foundation of China (82170905 to D.D.); the Program of Science and Technology Department of Sichuan Province (2024YFFK0153 to C.H.); the Project of Sichuan Provincial Administration of Traditional Chinese Medicine Innovation Research Team (2023ZD04 to Q.X.). These authors thank Fei Fu, Xiyu Wu, and Na Jiang from the Mass Spectrometry Center of Frontiers Science Center for Disease-related Molecular Network of West China Hospital, Sichuan University for helping with sample preparations; Liqiang Hu, Li Zhou, Jinhan Zhou, and Jingyao Zhang from Research Core Facility as well as Yue Li, Yi Zhang, and Li Li from the Institute of Clinical Pathology of West China Hospital for their help with histopathology examinations; and Xiaoting Chen from the Experimental Animal Center of West China Hospital, Sichuan University for helping with animal feeding. They also thank Chengdu Medical College for providing Discovery Studio software, and declare that the graphical abstract and some critical depicting images were created with BioRender.com.

Appendix A. Supplementary data

Supplementary data to this article can be found online at https://doi.org/10.1016/j.redox.2025.103900.

Data availability

Data will be made available on request.

References

[1] L. Boxhoorn, et al., Acute pancreatitis, Lancet 396 (10252) (2020) 726–734, https://doi.org/10.1016/S0140-6736(21)02377-1.
[2] P.J. Lee, G.I. Papachristou, New insights into acute pancreatitis, Nat. Rev. Gastroenterol. Hepatol. 16 (8) (2019) 479–496, https://doi.org/10.1038/s41575-019-0158-2.
[3] B.R. Stockwell, et al., Ferroptosis: a regulated cell death nexus linking metabolism, redox biology, and disease, Cell 171 (2) (2017) 273–285, https://doi.org/10.1016/j.cell.2017.09.021.
[4] Y. Peng, et al., Metabolomic-based clinical studies and murine models for acute pancreatitis disease: a review, Biochim. Biophys. Acta Mol. Basis Dis. 1867 (7) (2021) 166123, https://doi.org/10.1016/j.bbadis.2021.166123.
[5] M.M. Lerch, F.S. Gorelick, Models of acute and chronic pancreatitis, Gastroenterol. 144 (6) (2013) 1180–1193, https://doi.org/10.1053/j.gastro.2012.12.043.
[6] S.H. Rahman, A.R. Srinivasan, A. Nicolaou, Transsulfuration pathway defects and increased glutathione degradation in severe acute pancreatitis, Dig. Dis. Sci. 54 (3) (2008) 675–682, https://doi.org/10.1007/s10620-008-0382-z.
[7] S. Rius-Pérez, et al., Blockade of the trans-sulfuration pathway in acute pancreatitis due to nitration of cystathionine β-synthase, Redox Biol. 28 (2020) 101324, https://doi.org/10.1016/j.redox.2019.101324.
[8] S. Nishimura, et al., Hydrogen sulfide as a novel mediator for pancreatic pain in rodents, Gut 58 (6) (2009) 762–770, https://doi.org/10.1136/gut.2008.151910.
[9] K. Zuhra, et al., Cystathionine-β-synthase: molecular regulation and pharmacological inhibition, Biomolecules 10 (5) (2020) 697, https://doi.org/10.3390/biom10050697.
[10] J. Lin, et al., Effectiveness of Chengqi-series decoctions in treating severe acute pancreatitis: a systematic review and meta-analysis, Phytomedicine 113 (2023) 154727, https://doi.org/10.1016/j.phymed.2023.154727.
[11] Q. Qiu, et al., Rhei Radix et Rhizoma and its anthraquinone derivatives: potential candidates for pancreatitis treatment, Phytomedicine 129 (2024) 155708, https://doi.org/10.1016/j.phymed.2024.155708.
[12] R. Deng, et al., Properties and molecular mechanisms underlying geniposide-mediated therapeutic effects in chronic inflammatory diseases, J. Ethnopharmacol. 273 (2021) 113958, https://doi.org/10.1016/j.jep.2021.113958.
[13] G. Liang, et al., A multi-strategy platform for quality control and Q-markers screen of chaiqin chengqi decoction, Phytomedicine 85 (2021) 153525, https://doi.org/10.1016/j.phymed.2021.153525.
[14] Y. Huang, et al., Temporal metabolic trajectory analyzed by LC-MS/MS based targeted metabolomics in acute pancreatitis pathogenesis and chaiqin chengqi decoction therapy, Phytomedicine 99 (2022) 153996, https://doi.org/10.1016/j.phymed.2022.153996.
[15] G.S. Collins, et al., Transparent reporting of a multivariable prediction model for individual prognosis or diagnosis (TRIPOD): the TRIPOD statement, BMJ 350 (2015) g7594, https://doi.org/10.1136/bmj.g7594.

[16] W.Y. Du, et al., A microRNA checkpoint for Ca^{2+} signaling and overload in acute pancreatitis, Mol. Ther. 30 (4) (2022) 1754–1774, https://doi.org/10.1016/j.ymthe.2022.01.033.

[17] J.X. Yang, et al., Multi-dimensional metabolomic profiling reveals dysregulated ornithine metabolism hallmarks associated with a severe acute pancreatitis phenotype, Transl. Res. 263 (2024) 28–44, https://doi.org/10.1016/j.trsl.2023.08.003.

[18] P.A. Banks, et al., Classification of acute pancreatitis–2012: revision of the Atlanta classification and definitions by international consensus, Gut 62 (1) (2013) 102–111, https://doi.org/10.1136/gutjnl-2012-302779.

[19] Y.J. Wen, et al., Chaiqin chengqi decoction alleviates severity of acute pancreatitis via inhibition of TLR4 and NLRP3 inflammasome: identification of bioactive ingredients via pharmacological sub-network analysis and experimental validation, Phytomedicine 79 (2020) 153328, https://doi.org/10.1016/j.phymed.2020.153328.

[20] X.L. Ou, et al., Circulating histone levels reflect disease severity in animal models of acute pancreatitis, Pancreas 44 (7) (2015) 1089–1095, https://doi.org/10.1097/MPA.0000000000000416.

[21] H.T. Ma, et al., Endothelial transferrin receptor 1 contributes to thrombogenesis through cascade ferroptosis, Redox Biol. 70 (2024) 103041, https://doi.org/10.1016/j.redox.2024.103041.

[22] D. Du, et al., Protective effects of flavonoids from Coreopsis tinctoria nutt. on experimental acute pancreatitis via Nrf-2/ARE-mediated antioxidant pathways, J. Ethnopharmacol. 224 (2018) 261–272, https://doi.org/10.1016/j.jep.2018.06.003.

[23] J. Rong, et al., Inhibition of xanthine oxidase alleviated pancreatic necrosis *via* HIF-1α-regulated LDHA and NLRP3 signaling pathway in acute pancreatitis, Acta Pharm. Sin. B 14 (8) (2024) 3591–3604, https://doi.org/10.1016/j.apsb.2024.04.019.

[24] P. Heinrich, et al., Correcting for natural isotope abundance and tracer impurity in MS-, MS/MS- and high-resolution-multiple-tracer-data from stable isotope labeling experiments with IsoCorrectoR, Sci. Rep. 8 (1) (2018) 17910, https://doi.org/10.1038/s41598-018-36293-4.

[25] V. Kery, L. Poneleit, J.P. Kraus, Trypsin cleavage of human cystathionine beta-synthase into an evolutionarily conserved active core: structural and functional consequences, Arch. Biochem. Biophys. 355 (2) (1998) 222–232, https://doi.org/10.1006/abbi.1998.0723.

[26] D.J. Yan, et al., Flavin-dependent monooxygenase-mediated 1,2-oxazine construction *via* meisenheimer rearrangement in the biosynthesis of paeciloxazine, J. Am. Chem. Soc. 144 (9) (2022) 4269–4276, https://doi.org/10.1021/jacs.2c00881.

[27] M. Habib, et al., Ultrasonication modifies the structural, thermal and functional properties of pumpkin seed protein isolate (PSPI), Ultrason. Sonochem. 112 (2025) 107172, https://doi.org/10.1016/j.ultsonch.2024.107172.

[28] R. Yan, et al., Liquidambaric acid inhibits Wnt/β-catenin signaling and colon cancer via targeting TNF receptor-associated factor 2, Cell Rep. 38 (5) (2022) 110319, https://doi.org/10.1016/j.celrep.2022.110319.

[29] F. Cao, et al., Chaiqin chengqi decoction alleviates acute pancreatitis by targeting gasdermin D-mediated pyroptosis, J. Ethnopharmacol. 318 (Pt A) (2024) 116920, https://doi.org/10.1016/j.jep.2023.116920.

[30] J.B. Owen, D.A. Butterfield, Measurement of oxidized/reduced glutathione ratio, Methods Mol. Biol. 648 (2010) 269–277, https://doi.org/10.1007/978-1-60761-756-3_18.

[31] H.R. Zhu, et al., Cystathionine β-synthase in physiology and cancer, BioMed Res. Int. 2018 (2018) 3205125, https://doi.org/10.1155/2018/3205125.

[32] F. Skovby, J.P. Kraus, L.E. Rosenberg, Biosynthesis and proteolytic activation of cystathionine beta-synthase in rat liver, J. Biol. Chem. 259 (1) (1984) 588–593.

[33] M. Meier, et al., Structure of human cystathionine beta-synthase: a unique pyridoxal 5'-phosphate-dependent heme protein, EMBO J. 20 (15) (2001) 3910–3916, https://doi.org/10.1093/emboj/20.15.3910.

[34] C. Quijano, et al., Interplay between oxidant species and energy metabolism, Redox Biol. 8 (2016) 28–42, https://doi.org/10.1016/j.redox.2015.11.010.

[35] M. Hirota, et al., Relationship between plasma cytokine concentration and multiple organ failure in patients with acute pancreatitis, Pancreas 21 (2) (2000) 141–146, https://doi.org/10.1097/00006676-200008000-00006.

[36] X.F. Zhang, T.S. Gao, Y.H. Wang, Geniposide alleviates lipopolysaccharide (LPS)-induced inflammation by downregulation of miR-27a in rat pancreatic acinar cell AR42J, Biol. Chem. 400 (8) (2019) 1059–1068, https://doi.org/10.1515/hsz-2018-0422.

[37] J. Sastre, et al., Redox signaling in the pancreas in health and disease, Physiol. Rev. 105 (2) (2025) 593–650, https://doi.org/10.1152/physrev.00044.2023.

[38] L.J. Yang, et al., Effect of L-cysteine on remote organ injury in rats with severe acute pancreatitis induced by bile-pancreatic duct obstruction, hepatobiliary pancreat, Dis. Int. 12 (4) (2013) 428–435, https://doi.org/10.1016/s1499-3872(13)60067-3.

[39] D.A. Dickinson, H.J. Forman, Cellular glutathione and thiols metabolism, Biochem. Pharmacol. 64 (5–6) (2002) 1019–1026, https://doi.org/10.1016/s0006-2952(02)01172-3.

[40] E. Mosharov, M.R. Cranford, R. Banerjee, The quantitatively important relationship between homocysteine metabolism and glutathione synthesis by the transsulfuration pathway and its regulation by redox changes, Biochemistry 39 (42) (2000) 13005–13011, https://doi.org/10.1021/bi001088w.

[41] J.J. Zhu, et al., Transsulfuration activity can support cell growth upon extracellular cysteine limitation, Cell Metab. 30 (5) (2019) 865–876.e5, https://doi.org/10.1016/j.cmet.2019.09.009.

[42] J.I. Sbodio, S.H. Snyder, B.D. Paul, Regulators of the transsulfuration pathway, Br. J. Pharmacol. 176 (4) (2019) 583–593, https://doi.org/10.1111/bph.14446.

[43] A. Kumar, M. Bhatia, Role of hydrogen sulfide, substance P and adhesion molecules in acute pancreatitis, Int. J. Mol. Sci. 22 (22) (2021) 12136, https://doi.org/10.3390/ijms222212136.

[44] T.J. McCorvie, et al., Architecture and regulation of filamentous human cystathionine beta-synthase, Nat. Commun. 15 (1) (2024) 2931, https://doi.org/10.1038/s41467-024-46864-x.

[45] L. Celano, et al., Inactivation of cystathionine beta-synthase with peroxynitrite, Arch. Biochem. Biophys. 491 (1–2) (2009) 96–105, https://doi.org/10.1016/j.abb.2009.08.022.

[46] S. Bruno, et al., Functional properties of the active core of human cystathionine beta-synthase crystals, J. Biol. Chem. 276 (1) (2001) 16–19, https://doi.org/10.1074/jbc.C000588200.

[47] E. Mijatovic, et al., Cellular turnover and degradation of the Most common missense cystathionine beta-synthase variants causing homocystinuria, Protein Sci. 33 (8) (2024) e5123, https://doi.org/10.1002/pro.5123.

[48] A. Saluja, et al., Early intra-acinar events in pathogenesis of pancreatitis, Gastroenterol. 156 (7) (2019) 1979–1993, https://doi.org/10.1053/j.gastro.2019.01.268.

[49] M. Hirota, M. Ohmuraya, H. Baba, The role of trypsin, trypsin inhibitor, and trypsin receptor in the onset and aggravation of pancreatitis, J. Gastroenterol. 41 (9) (2006) 832–836, https://doi.org/10.1007/s00535-006-1874-2.

[50] A.S. Gukovskaya, et al., Recent insights into the pathogenic mechanism of pancreatitis: role of acinar cell organelle disorders, Pancreas 48 (4) (2019) 459–470, https://doi.org/10.1097/MPA.0000000000001298.

[51] M. Hirota, et al., Roles of autophagy and pancreatic secretory trypsin inhibitor in trypsinogen activation in acute pancreatitis, Pancreas 49 (4) (2020) 493–497, https://doi.org/10.1097/MPA.0000000000001519.

[52] H.Y. Gaisano, et al., Supramaximal cholecystokinin displaces Munc18c from the pancreatic acinar basal surface, redirecting apical exocytosis to the basal membrane, J. Clin. Investig. 108 (11) (2001) 1597–1611, https://doi.org/10.1172/JCI9110.

[53] M.A. Manso, et al., Changes in both the membrane and the enzyme content of individual zymogen granules are associated with sodium taurocholate-induced pancreatitis in rats, Clin. Sci (Lond). 94 (3) (1998) 293–301, https://doi.org/10.1042/cs0940293.

[54] M.L. Steer, J. Meldolesi, The cell biology of experimental pancreatitis, N. Engl. J. Med. 316 (3) (1987) 144–150, https://doi.org/10.1056/NEJM198701153160306.

[55] Y.J. Jia, M.N. Jiang, J.T. Gao, Protective effect of fructus gardeniae on pancreatic subcellular organs of the acute pancreatitis in rats, Zhongguo Zhong Xi Yi Jie He Za Zhi 16 (6) (1996) 355–357. Chinese.

[56] A. Meister, Glutathione deficiency produced by inhibition of its synthesis, and its reversal; applications in research and therapy, Pharmacol. Ther. 51 (2) (1991) 155–194, https://doi.org/10.1016/0163-7258(91)90076-x.

[57] R. Lüthen, et al., Trypsinogen activation and glutathione content are linked to pancreatic injury in models of biliary acute pancreatitis, Int. J. Pancreatol. 24 (3) (1998) 193–202, https://doi.org/10.1007/BF02788422.

[58] J. Li, et al., Perspectives of traditional Chinese medicine in pancreas protection for acute pancreatitis, World J. Gastroenterol. 23 (20) (2017) 3615–3623, https://doi.org/10.3748/wjg.v23.i20.3615.

[59] X.P. Zhang, D.R. Liu, Y. Shi, Study progress in therapeutic effects of traditional Chinese medicine monomer in severe acute pancreatitis, J. Zhejiang Univ. Sci. B 8 (2) (2007) 147–152, https://doi.org/10.1631/jzus.2007.B0147.

[60] X. Jiang, et al., Drug discovery and formulation development for acute pancreatitis, Drug Deliv. 27 (1) (2020) 1562–1580, https://doi.org/10.1080/10717544.2020.1840665.

[61] T. Seta, et al., Treatment of acute pancreatitis with protease inhibitors administered through intravenous infusion: an updated systematic review and meta-analysis, BMC Gastroenterol. 14 (2014) 102, https://doi.org/10.1186/1471-230X-14-102.

[62] R. Banerjee, Catalytic promiscuity and heme-dependent redox regulation of H2S synthesis, Curr. Opin. Chem. Biol. 37 (2017) 115–121, https://doi.org/10.1016/j.cbpa.2017.02.021.